

# Experimental bounds on sterile-active neutrino mixing angles









#### **THESIS**

submitted in partial fulfillment of the requirements for the degree of

> MASTER OF SCIENCE in THEORETICAL PHYSICS

Author: Mihael Petač Student ID: 1446290 Supervisor: Dr. Alexey Boyarsky  $2^{nd}$  corrector: Dr. Dorothea Samtleben

Leiden, The Netherlands, June 30, 2015

# Experimental bounds on sterile-active neutrino mixing angles

#### Mihael Petač

Instituut-Lorentz, Leiden University P.O. Box 9500, 2300 RA Leiden, The Netherlands

June 30, 2015

#### **Abstract**

Despite the success of the Standard Model in the last few decades, we know it is not complete. There is strong motivation for assuming the existence of aditional heavy neutral leptons, which can account for active neutrino masses and possibly also have cosmological implications. In this work I consider the Standard Model with two neutral lepton singlets (sterile neutrinos) with degenerated masses in the range 20MeV - 2GeV. The constraints on the active-sterile neutrino mixing angles are evaluated based on recent neutrino oscillations data. Using these constraints the bounds from accelerator experiments are reanalyzed for the case of the considered model. Finally, the results are compared with cosmological constraints coming from Big Bang nucleosynthesis and the  $\nu MSM$  resonant leptogenesis.

# Contents

1	Introduction			
2	Ste	ile neutrinos	5	
	2.1	Sterile neutrinos and the Standard Model		
	2.2	The see-saw mechanism	6 8 9	
	2.3	Sterile-active neutrino mixing angles	ç	
3	Net	itrino oscillations	13	
	3.1	Theoretical background	14	
	3.2	Experiments	15	
		3.2.1 Solar and long baseline reactor experiments	16	
		3.2.2 Atmospheric and accelerator experiments	19	
		3.2.3 Short baseline reactor experiments	22	
	3.3	Bounds on neutrino oscillation parameters	23	
		3.3.1 NuFIT results	23	
	3.4	Bounds on sterile-active neutrino mixing angles	27	
		3.4.1 Evaluation	27	
		3.4.2 Results	28	
4	Dir	ect detection searches	31	
	4.1	Peak search experiments	32	
	4.2	Beam dump experiments	32	
		Combined direct detection bounds	38	
5	Cos	mological constraints	43	
	5.1	Big Bang nucleosynthesis	44	
	5.2	Resonant leptogenesis	45	
6	Con	iclusions	47	

vi CONTENTS

A	Chi-squared test			51
В	Scat	tering	processes involving sterile neutrino	55
		_	e neutrino decays	56
		B.1.1	Three body decay modes	56
		B.1.2	Two body decay modes	60
	B.2	Sterile	e neutrino production	65
			Pure leptonic meson decays	65
			Semi-leptonic meson decays	66

	<u> </u>			
	<b>4</b>			
I				
'				
Chapter				
Onapio	_			

# Introduction

In the recent decades we have witnessed numerous advances in theoretical physics, broadening our understanding of the Universe from the smallest to the largest scales. One of the most prominent examples is the establishment of the Standard Model, which describes interactions of the fundamental particles with staggering accuracy. When it was proposed, it predicted new particles which have all been successfully found in later accelerator experiments. The final confirmation came in 2013, when the Higgs boson was detected, making the Standard Model complete and selfconsistent. Cosmology, dealing with the largest scales in the Universe, also witnessed rapid advances in the recent past. Thanks to precise observations phenomena like dark matter and dark energy have been established. Moreover, successful theoretical model for describing the evolution of the Universe from the very first moments all the way to the present was developed, known as the Big Bang theory. Its consistency with the Standard Model was confirmed by cosmic microwave background observations (e.g. the baryon acoustic oscillations). Furthermore, an important bridge between the two fields is the Big Bang nucleosynthesis, a theory which describes creation of first atomic nuclei from primordial plasma. The abundances of produced elements strongly depend on particle physics and cosmology, therefore the excellent agreement with observations speaks strongly in favor of these two models.

Despite all the success, there are still phenomena which do not fit in the framework of current theories. For example, there is no candidate for dark matter particle within the Standard Model, but on the other hand we know that it constitutes majority of the Universe's matter component. We also lack the understanding of how the baryon asymmetry of the Universe was generated and what is driving the accelerated expansion. The Stan2 Introduction

dard Model actually fails even in describing all known fundamental particles, since neutrinos are assumed to be massless, which is in contradiction with well established phenomena of neutrino oscillations This arguments lead to different proposed extensions of the Standard Model, which could resolve one or more of the problems and not spoil the experimentally confirmed predictions. Examples of such extensions are the super-symmetric theories, which predict the existence of multiple partners of the Standard Model particles. The additional super-symmetric particles have been systematically searched for in accelerator experiments with no positive result so far. An alternative approach is to assume existence of extremely weakly interacting particles within the current Standard Model. Very appealing candidates for such particles are the sterile neutrinos, which can in some models account for neutrino oscillations, dark matter and baryon asymmetry at the same time. Furthermore, such sterile neutrinos could be detected by proposed accelerator experiments allowing for conclusive results in near future.

The aim of my project was to study sterile neutrinos, in particular a model of two sterile neutrinos in GeV mass range. This is an interesting choice, because it can give an explanation to the neutrino oscillations and origin of baryon asymmetry. Furthermore, results obtained in this thesis are also applicable to other models, e.g. the  $\nu$ MSM which contains additional sterile neutrino neutrino in keV mass range, being the dark matter candidate. Since the considered model attempts to explain various phenomena, we can use independent observations to constrain it. In this work I use the bounds coming from neutrino oscillations and direct detection experiments to compute upper bound on coupling strength and lower bound on lifetime of sterile neutrinos. In addition to that I compare my results with cosmological constrains.

An introduction to sterile neutrinos and their properties is given in Chapter 2. Additionally, their role in the Standard Model is discussed, followed by an explanation of the see-saw mechanism and definition of the sterile-active neutrino mixing angles. Chapter 3 is devoted to neutrino oscillations. First the theoretical background is discussed, which is followed by an overview of the most important neutrino oscillation experiments. Finally the bounds on sterile-active neutrino mixing angle ratios, based on the neutrino oscillation, are derived. In Chapter 4 the constraints on sterile neutrinos, that come from accelerator direct detection experiments are presented. The two most important types of experiments for the  $\mathcal{O}(\text{GeV})$  mass range, beam dump and peak searches, are considered. Some of the bounds from beam dump experiments are reinterpreted, since they can strengthened for the considered model. Cosmological constraint, applica-

ble to the two heavy neutrino states, are briefly reviewed in Chapter 5. In the final Chapter 6 the combination of all discussed bounds is presented.



# Sterile neutrinos

The Standard Model (SM) of particle physics is a theory describing the kinematics and interactions of the fundamental particles. The SM, as we know it today, was developed in the late 1960s by Steven Weinberg [1], Sheldon Glashow and Abdus Salam with the help of many other contributing scientists. It is based on mathematical framework of quantum field theory, where the behavior of the system is given by the Lagrangian. its symmetry under the U(1), SU(2) and SU(3) gauge groups gives rise to the electromagnetic, weak and strong interactions. The predictions of the SM have been thoroughly tested and agree with the experiments with staggering accuracy. This led to general acceptance of the SM and today it is considered the main theory of particle physics.

Despite all the success, there is a number of observed phenomena, which tell us that SM is not complete. For example, the neutrino oscillations imply that at least two neutrinos have non-zero masses, while they are assumed to be massless in the minimal SM. The neutrino masses can be included by adding a higher dimensional term  $\frac{1}{\Lambda}(\bar{L^C}\tilde{\Phi})(\tilde{\Phi}^TL)$ , with  $\Lambda$ being a dimensionful coupling constant, L the lepton doublet and  $\Phi$  the Higgs doublet. Such term would spoil the unitarity of the SM and make the theory non-renormalizable. However, the active neutrino masses are known to be less than few eV, therefore  $\Lambda \geq \mathcal{O}(10^{13} \text{ GeV})$ , which corresponds to energies where quantum field theory is expected to break down. Further reason why the SM can not be complete is the existence of the dark matter (DM). It has been shown that it constitutes a vast part of the matter content of the Universe and can not be constituted by any of the SM particles. There is also no mechanism that could have lead to the observed baryon asymmetry of the Universe (BAU). Even though there are CP violating processes and the baryon number is not strictly conserved in the 6 Sterile neutrinos

SM, these effects are too small and would be washed out by later thermal equilibrium. These problems can be addressed by assuming the existence of heavy neutral lepton singlets, sterile neutrinos. They are right-chiral neutral particles and therefore do not take part in any of the gauge interactions, making them suitable candidates for DM. By introducing two right-chiral neutrinos to the SM we can explain the neutrino oscillations and the smallness of active neutrino masses through the so called see-saw mechanism. Additionally, if they have degenerate masses greater than few hundred MeV they could account for BAU through the resonant leptogenesis. This gives us good motivation to consider such extensions of the SM, as they address multiple important problems at the same time. In this project I focus on a model with two sterile neutrinos with degenerated masses in the range between 20 MeV and 2 GeV. Such model is the minimal extension of the SM with sterile neutrinos that is capable of explaining neutrino masses and oscillation and providing a mechanism for generating the BAU. The particular mass range was considered, because it corresponds to the energies where the strongest constraints on heavy neutral lepton coupling strength were obtained.

In the first section 2.1 of this chapter I discuss the properties of sterile neutrinos and their role in the SM. In section 2.2 I will present the seesaw mechanism, which can explain the small active neutrino masses. In the final section 2.3 I will discuss the sterile-active neutrino mixing angles, which characterize the coupling strength between sterile and active neutrinos, and how they are constrained by the see-saw mechanism.

#### 2.1 Sterile neutrinos and the Standard Model

Sterile neutrinos are hypothetical neutral lepton singlets, which implies a number of interesting properties. First of all, they are not charged under any of the gauge interactions (zero charge under U(1) and singlets under SU(2) and SU(3) gauge groups) and therefore can not interact through electromagnetic, weak or strong force. As they are truly neutral particles, they must be invariant under particle-antiparticle conjugation, associated with operator  $\hat{C}: \Psi \to \Psi^{\mathcal{C}} = \mathcal{C}\bar{\Psi}^T$  where  $\Psi$  and  $\bar{\Psi}$  are the Dirac 4-spinor and its adjoint respectively and  $\mathcal{C}$  is an antisymmetric matrix which can be written in Weyl basis as  $\mathcal{C} = i\gamma^2\gamma^0$ . It turns out that fields which fulfill the condition  $\Psi^{\mathcal{C}} = \Psi$  are special solutions of Dirac equation, known as Majorana fermions, which obey the Majorana equation

$$-i\partial \Psi + m_M \Psi^{\mathcal{C}} = 0 \tag{2.1}$$

Here  $m_M$  is the Majorana mass, which does not arise from coupling with Higgs like Dirac masses. In Weyl basis it is easy to show that  $\Psi$  in (2.1) must take the following form

$$\Psi = \begin{pmatrix} \zeta \\ -i\sigma^2 \zeta^* \end{pmatrix} \tag{2.2}$$

where  $\zeta$  is a 2-spinor and  $\sigma^2$  the second Pauli matrix. From here we can see that a Majorana fermion can be fully described by a 2-spinor and not a 4-spinor, which is the case for charged fermions. For further discussion it is important to remember that sterile neutrinos are Majorana fermions, i.e. they are invariant under particle-antiparticle conjugation, and can have Majorana masses. A more thorough discussion about Majorana fermions can be found in [2]

In the context of the SM sterile neutrinos are right-chiral particles, as all other lepton and quark SU(2) singlets. They are often presented as counterparts to active neutrinos, which are always left-chiral. In analogy to other fermions in the SM, we can write down an interaction Lagrangian of the Yukawa type, coupling the sterile neutrinos to a left lepton doublet and Higgs field, which is responsible for mixing of active and sterile neutrinos. For sterile neutrinos we can also construct a Majorana mass term, which is absent in the SM since none of its particles are Majorana fermions. The most general SM Lagrangian including  $\mathcal N$  sterile neutrinos has the following form

$$\mathcal{L} = \mathcal{L}_{SM} + i\bar{N}_I \partial N_I - (F_{\alpha I}\bar{L}_{\alpha}N_I \tilde{\Phi} + \frac{M_{N,IJ}}{2}\bar{N}_I^c N_J + \text{h.c.})$$
 (2.3)

Here  $\mathcal{L}_{SM}$  is the Standard Model Lagrangian,  $N_I$  are the neutrino singlets  $(I, J = 1, ..., \mathcal{N})$ ,  $L_{\alpha}$  the lepton doublet  $(\alpha = e, \mu, \tau)$  and  $\Phi$  the Higgs doublet, where  $\tilde{\Phi} = i\sigma^2\Phi^*$ .  $\mathbf{F}$  is the Yukawa coupling matrix and  $\mathbf{M}_N$  the Majorana mass matrix. After the electroweak symmetry breaking lepton doublet and Higgs field become  $L_{\alpha} = \binom{v_{\alpha}}{l_{\alpha}}$  and  $\langle \Phi \rangle = \binom{0}{v/\sqrt{2}}$ , with  $\mathbf{M}_D = \mathbf{F} \frac{v}{\sqrt{2}}$  being the Dirac mass matrix.

The Neutrino Minimal Standard Model ( $\nu MSM$ ) [3] is a particularly attractive extension of the SM, which can explain the origin of neutrino masses and oscillations, gives a dark matter candidate and proposes a mechanism for generating the BAU. It is based on the Lagrangian (2.3) and assumes the existence of 3 sterile neutrinos,  $N_1$  in the keV mass range, while  $N_2$  and  $N_3$  must have nearly degenerate masses above  $\mathcal{O}(\text{MeV})$ . The light sterile neutrino plays the role of a DM candidate and must couple much weaker then the heavier two states. In fact, the absence of any kind

8 Sterile neutrinos

of DM decay signal implies that lifetime, inversely proportional to the coupling strength, must be many orders of magnitude larger then the Hubble time. Such sterile neutrinos could not explain the neutrino oscillations or be observed in accelerators and are therefore neglected in the analysis of laboratory experimental. The two heavy sterile neutrinos must be coupled stronger, however still very weakly compared to other particles in the SM. In order to explain the neutrino oscillations lower bound on the mixing angles between active and sterile neutrinos can be derived through the see-saw mechanism. If the heavy sterile neutrinos have degenerate masses they could effectively generate the BAU through resonant leptogenesis, which has been shown to be possible for masses down to MeV range [3, 4]. I will discuss this in Chapter 5 along with the effect of sterile neutrinos on Big Bang nucleosynthesis. Such heavy neutral leptons have been searched in numerous accelerator experiments, however no events that could be associated with them were ever found. This allows us to establish upper bound on their coupling strength and will be discussed more in detail in Chapter 4.

#### 2.2 The see-saw mechanism

An important feature of sterile neutrinos is that they can explain neutrino masses and oscillations. This is achieved by additional Yukawa coupling of active neutrinos to sterile neutrinos and Higgs, generating the Dirac masses. Furthermore, the existence of Majorana mass term can explain the smallness of active neutrino masses through the see-saw mechanism. This can be seen by considering the additional mass terms in the Lagrangian (2.3), which become after the electroweak symmetry breaking

$$\mathcal{L}_{mass} = -M_{D,\alpha I} \bar{\nu}_{\alpha} N_I - \frac{M_{N,IJ}}{2} \bar{N}_I^c N_J + \text{h.c.}$$
 (2.4)

Such Lagrangian is written in gauge (flavor) basis, which is the eigenbasis of weak interactions and does not necessarily coincide with mass eigenbasis. In fact, there must be a non-trivial unitary transformation  $\mathbf{U}$  (the PMNS matrix) between the two bases for the theory to explain the neutrino oscillations, discussed more in detail in Section 3.1. The sterile neutrinos states can be assumed as Majorana mass eigenstates, making  $M_N$  diagonal, without loss of generality [3]. Defining the following column

$$\Psi = \begin{pmatrix} \bar{\boldsymbol{\nu}}^{\mathcal{C}} \\ \mathbf{N} \end{pmatrix} \tag{2.5}$$

where v is a vector of all active neutrino states and N a vector of all sterile neutrino states. The corresponding Lagrangian and mass matrix are

$$\mathcal{L} = \frac{1}{2} \bar{\Psi}^{C} \mathcal{M} \Psi + \text{h.c.} \quad , \quad \mathcal{M} = \begin{pmatrix} 0 & \mathbf{M}_{D} \\ \mathbf{M}_{D}^{T} & \mathbf{M}_{N} \end{pmatrix}$$
 (2.6)

This allows us to diagonalize matrix  $\mathcal{M}$  and obtain the neutrino mass eigenbasis. Assuming that Dirac masses are much smaller then Majorana masses, i.e.  $|M_D| \ll |M_N|$ , which is essential for explaining the smallness of active neutrino masses and weakness of sterile neutrino coupling, the diagonalized matrix  $\mathcal{M}$  takes the following form

$$\hat{\mathcal{M}} = \begin{pmatrix} \mathbf{m}_{\nu} & 0\\ 0 & \mathbf{m}_{N} \end{pmatrix} \tag{2.7a}$$

$$\mathbf{m}_N = \mathbf{M}_N + \mathcal{O}(\mathbf{M}_D \mathbf{M}_N^{-1}) \tag{2.7b}$$

$$\mathbf{m}_{\nu} = -\mathbf{M}_{D}\mathbf{M}_{N}^{-1}\mathbf{M}_{D}^{T} \tag{2.7c}$$

Here the  $\mathbf{m}_N$  is the sterile neutrino mass matrix, which coincides with  $\mathbf{M}_N$  to the first order in  $\mathbf{M}_D\mathbf{M}_N^{-1}$ , and  $\mathbf{m}_\nu$  the active neutrino mass matrix. An important consequence is that active neutrino masses are small under the assumption  $|\mathbf{M}_D| \ll |\mathbf{M}_N|$ . Additionally, the experimental evidence for two mass splittings in active neutrino masses, discussed in Section 3.2, implies that the rank of active neutrino mass matrix  $\mathcal{R}[\mathbf{m}_\nu]$  is equal to or greater than 2. From Equation (2.7c) follows

$$\mathcal{R}[\mathbf{m}_{\nu}] = \mathcal{R}[\mathbf{M}_{D}\mathbf{M}_{N}^{-1}\mathbf{M}_{D}^{T}] = \mathcal{R}[\mathbf{M}_{N}] \ge 2$$
 (2.8)

which means that at least two sterile neutrinos are needed to explain active neutrinos masses and oscillations. Therefore, in what follows, the existence of two sterile neutrinos will be assumed ( $\mathcal{N}=2$ ).

## 2.3 Sterile-active neutrino mixing angles

As already discussed in beginning of the chapter, sterile neutrinos do not take part in electromagnetic, weak or strong interactions. However, they do couple to active neutrinos and the strength of this interaction can be parametrized by the sterile-active neutrino mixing angles, for which I will use the following definition

$$\vartheta_{\alpha}^{2} = \frac{1}{2} \sum_{I} |(\mathbf{M}_{D} \mathbf{M}_{N}^{-1})_{\alpha I}|^{2}$$
 (2.9)

10 Sterile neutrinos

The mixing angles are essentially the rotation angles between active neutrino flavor states and sterile neutrino states. In the case of this project I used definition (2.9), where the sterile neutrino mass states are averaged over, since they are assumed to be mass degenerate, therefore  $\mathbf{M}_N = \mathbb{1}_2 M_N$ . The square of the mixing angle is equal to the probability for a sterile neutrino to oscillate into an active neutrino (or the other way around). This kind of process violates the conservation of lepton flavors and is most likely CP violating. The corresponding Feynman diagram is shown in Figure 2.1

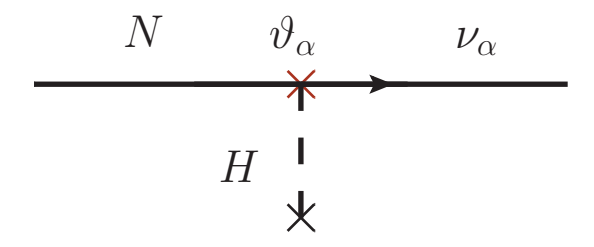


**Figure 2.1:** Feynman diagram corresponding to the Yukawa interaction term in the Lagrangian (2.3)

Using the PMNS matrix **U** (3.2) we can diagonalize the active neutrino mass matrix  $\mathbf{m}_{\nu}$ 

$$\operatorname{diag}(m_1 e^{-2i\zeta}, m_2 e^{-2i\xi}, m_3) = \mathbf{U}^T \mathbf{m}_{\nu} \mathbf{U}$$
 (2.10)

where  $\zeta$  and  $\xi$  are the Majorana phases, which arise due to Majorana mass term and can not be determined through oscillation experiments, unlike the PMNS parameters and the active neutrino mass splittings. We can rewrite this using the see-saw formula (2.7c), which in case of two sterile neutrinos yields

diag
$$(m_1 e^{-2i\zeta}, m_2 e^{-2i\xi}, m_3)_{ij} = -\frac{\tilde{M}_{D,i2}\tilde{M}_{D,j3} + \tilde{M}_{D,i3}\tilde{M}_{D,j2}}{M_N}$$
 (2.11)  
 $\tilde{\mathbf{M}}_D = \mathbf{U}^T \mathbf{M}_D$ 

Here it is important to notice that (2.11) is invariant under  $(\tilde{M}_{D,i2}, \tilde{M}_{D,j3}) \rightarrow (z\tilde{M}_{D,i2}, z^{-1}\tilde{M}_{D,j3})$ , which gives us another free complex-valued parameter z, which is related to the ratio between Yukawa coupling constants of  $N_2$  and  $N_3$ . In the considered model, with two sterile neutrinos, only two active neutrinos can have non-zero masses, since  $\mathcal{R}[\mathbf{m}_{\nu}] = \mathcal{R}[\mathbf{M}_N] = 2$ .

This implies  $m_1 = 0$  for normal hierarchy (NH) and  $m_3 = 0$  for inverted hierarchy (IH). Using the above, we can solve (2.9) explicitly for NH

$$\vartheta_{\alpha}^{2} = \frac{|z|^{2}}{4M_{N}} \left( \left| \sqrt{m_{3}} U_{\alpha 3} - i e^{i\xi} \sqrt{m_{2}} U_{\alpha 2} \right|^{2} + \frac{1}{|z|^{4}} \left| \sqrt{m_{3}} U_{\alpha 3} + i e^{i\xi} \sqrt{m_{2}} U_{\alpha 2} \right|^{2} \right)$$
(2.12)

and for IH

$$\vartheta_{\alpha}^{2} = \frac{|z|^{2}}{4M_{N}} \left( \left| \sqrt{m_{1}} U_{\alpha 1} - i e^{i(\xi - \zeta)} \sqrt{m_{2}} U_{\alpha 2} \right|^{2} + \frac{1}{|z|^{4}} \left| \sqrt{m_{1}} U_{\alpha 1} + i e^{i(\xi - \zeta)} \sqrt{m_{2}} U_{\alpha 2} \right|^{2} \right)$$
(2.13)

From (2.12) and (2.13) we see that the mixing angles are not uniquely determined even if we fix the sterile neutrino mass  $M_N$ . For successful baryogenesis in the  $\nu$ MSM we get a constrain on z [5], being  $|z|^2 \gg 1$ , so we can neglect the term proportional to  $|z|^{-4}$ .

It turns out to be useful to define the mixing angle ratio

$$T_{\alpha} = \frac{\vartheta_{\alpha}^2}{\sum_{\beta} \vartheta_{\beta}^2} \tag{2.14}$$

where the sum in denominator, due to unitarity of **U**, equals to

$$\sum_{\beta} \vartheta_{\beta}^{2} = \frac{|z|^{2}}{4M_{S}} (m_{2} + m_{3}) \quad \text{for NH}$$
 (2.15)

$$\sum_{\beta} \vartheta_{\beta}^{2} = \frac{|z|^{2}}{4M_{S}} (m_{1} + m_{2}) \quad \text{for IH}$$
 (2.16)

Together with (2.12) and (2.13) this gives us the following expression for the mixing angle ratios

$$T_{\alpha}^{NH} = \frac{1}{1 + \frac{m_2}{m_3}} \left( \left| U_{\alpha 3} - i e^{i\xi} \sqrt{\frac{m_2}{m_3}} U_{\alpha 2} \right|^2 \right)$$
 (2.17)

$$T_{\alpha}^{IH} = \frac{1}{1 + \frac{m_2}{m_1}} \left( \left| U_{\alpha 1} - i e^{i(\xi - \zeta)} \sqrt{\frac{m_2}{m_1}} U_{\alpha 2} \right|^2 \right)$$
 (2.18)

It can be immediately seen, that these expressions do not depend on  $M_N$  and z anymore, but only on the PMNS parameters, active neutrino masses

12 Sterile neutrinos

and Majorana phases. All of these quantities, except the Majorana phases  $\zeta$  and  $\xi$ , can be determined through neutrino oscillation experiments (under assumption that lightest active neutrino has zero or negligible mass). Therefore, we can improve the bounds on mixing angles with preciser measurements of neutrino oscillations. However, the unconstrained Majorana phases turn out to be the main source of uncertainty, as will be shown in the neutrino oscillation data analysis in Section 3.4.



The first clue for neutrino oscillations was discovered by Ray Davis' Homestake experiment in 1965. It was designed to measure solar neutrino flux through  $v_e + {}^{37}Cl \rightarrow {}^{37}Ar^+ + e^-$  reaction. The obtained results were a big surprise, since they measured only one third of the flux predicted by the standard solar models of the time. The Homestake experiment was followed by many other experiments, such as Kamiokande in Japan, SAGE in the former Soviet Union, GALLEX in Italy and SNO in Ontario, Canada. They all measured deficit of electron neutrinos, which lead to establishment of neutrino oscillations. Already in 1957 B. Pontecorvo [6] proposed a mechanism for neutrino oscillations, similar to the one in the strong sector, responsible for neutral kaon mixing. The idea behind it is, that neutrinos interact through weak force in their flavor (also referred to as gauge) eigenstates, which are a superposition of the mass eigenstates. However, neutrinos propagate through vacuum as mass eigenstates, which pick up different phases from having different masses, resulting in flavor mixing. This explains the measured deficit of  $\nu_e$  coming from the sun, since part of them oscillates in other flavors, while traveling to earth. As already discussed, the existence of sterile neutrinos could explain the origin of neutrino masses and oscillations. Therefore bounds on sterile-active mixing angles can be imposed, based on oscillation experiments.

In the first section 3.1 of this chapter I discuss the theoretical background of the neutrino oscillations and derive the expression for the oscillation probabilities. This is followed by section 3.2, which contains a review of neutrino oscillation experiments. In section 3.3 I present the most recent constraints on the neutrino oscillation parameters, coming from the combination of the most successful experiments. These constraints can be used to fix the minimal and maximal values of the mixing angle ratios as

has been shown in the previous chapter. In the final section 3.4 I discuss the evaluation of the bounds of mixing angle ratios and present the obtained results.

## 3.1 Theoretical background

The unitary transformation, postulated by B. Pontecorvo, that relates the flavor to mass eigenbasis, is the Pontecorvo-Maki-Nakagawa-Sakata (PMNS) matrix **U**. One can use it to transform between flavor  $|\nu_{\alpha}\rangle$  (with  $\alpha = e$ ,  $\mu$ ,  $\tau$ ) and mass eignestates  $|\nu_{i}\rangle$  (with i = 1, 2, 3) in the following way

$$|\nu_i\rangle = \sum_{\alpha} U_{\alpha i} |\nu_{\alpha}\rangle \tag{3.1a}$$

$$|\nu_{\alpha}\rangle = \sum_{i} U_{\alpha i}^{*} |\nu_{i}\rangle \tag{3.1b}$$

The PMNS matrix is a  $3 \times 3$  unitary matrix, which has in general 9 real parameters. However, by redefining the fields we can eliminate 5, which leaves us with 3 rotation angles  $\theta_{12}$ ,  $\theta_{13}$ ,  $\theta_{23}$  and one CP violating phase  $\delta_{CP}$ . It is usually parameterized as

$$U = \begin{pmatrix} 1 & 0 & 0 \\ 0 & c_{23} & s_{23} \\ 0 & -s_{23} & c_{23} \end{pmatrix} \begin{pmatrix} c_{13} & 0 & s_{13} \\ 0 & e^{i\delta_{CP}} & 0 \\ -s_{13} & 0 & c_{13} \end{pmatrix} \begin{pmatrix} c_{12} & s_{12} & 0 \\ -s_{12} & c_{12} & 0 \\ 0 & 0 & 1 \end{pmatrix}$$

$$= \begin{pmatrix} c_{12}c_{13} & c_{13}s_{12} & s_{13} \\ -c_{23}s_{12}e^{i\delta_{CP}} - c_{12}s_{13}s_{23} & c_{12}c_{23}e^{i\delta_{CP}} - s_{12}s_{13}s_{23} & c_{13}s_{23} \\ s_{23}s_{12}e^{i\delta_{CP}} - c_{12}c_{23}s_{13} & -c_{12}s_{23}e^{i\delta_{CP}} - c_{23}s_{12}s_{13} & c_{13}c_{23} \end{pmatrix}$$

$$(3.2)$$

where  $s_{ij} = \sin \theta_{ij}$  and  $c_{ij} = \cos \theta_{ij}$ .

As I mentioned before, neutrinos propagate through vacuum in mass eigenstates, i.e. the mass basis diagonalizes the free Hamiltonian. We can write the time evolution of a free neutrino as follows:

$$|\nu_i(t)\rangle = e^{-i\hat{H}t}|\nu_i(0)\rangle = e^{-iE_it}|\nu_i(0)\rangle$$
(3.3)

For shorter notation, I will denote  $|\nu(0)\rangle = |\nu\rangle$  in the rest of the text. Since  $|\nu_{\alpha}\rangle$  is a linear combination of  $|\nu_{i}\rangle$ , and each mass eigenstate has its own time evolution, the probability to measure a certain flavor also evolves with time. Using this, we can calculate the transition amplitude between

3.2 Experiments 15

different flavor states

$$A(\nu_{\alpha} \to \nu_{\beta}; t) = \langle \nu_{\beta}(t) | \nu_{\alpha} \rangle = \sum_{i} \langle \nu_{\beta} | e^{i\hat{H}t} | \nu_{i} \rangle \langle \nu_{i} | \nu_{\alpha} \rangle =$$

$$= \sum_{i} \left( \sum_{j} \langle \nu_{j} | (U_{j\beta}^{*})^{\dagger} e^{iE_{i}t} | \nu_{i} \rangle \right) \left( \langle \nu_{i} | \sum_{j} U_{\alpha j}^{*} | \nu_{j} \rangle \right) =$$

$$= \sum_{i} e^{iE_{i}t} U_{\beta i} U_{\alpha i}^{*}$$
(3.4)

In the last step of calculation the orthogonality of the states,  $\langle v_i | v_j \rangle = \delta_{i,j}$  was used. The probability for oscillation between two flavors is given by the absolute square of the transition amplitude, which yields

$$P(\nu_{\alpha} \to \nu_{\beta}) = |A(\nu_{\alpha} \to \nu_{\beta})|^{2} =$$

$$= \delta_{\alpha,\beta} - 4 \sum_{j>i} Re[U_{\alpha j}^{*} U_{\beta j} U_{\alpha i} U_{\beta i}^{*}] \sin^{2}(\frac{\Delta m_{ji}^{2}}{4E} L)$$

$$+ 2 \sum_{j>i} Im[U_{\alpha j}^{*} U_{\beta j} U_{\alpha i} U_{\beta i}^{*}] \sin(\frac{\Delta m_{ji}^{2}}{2E} L)$$
(3.5)

In this derivation we assume neutrinos to be ultra relativistic ( $E\gg m$ ) and denote  $\Delta m_{ji}^2=m_j^2-m_i^2$ . The obtained expression turns out to be very practical for interpreting experimental results, since we usually have information about the energy of neutrinos and the distance they traveled. Also, it is useful to write the imaginary term separately, since it is responsible for the CP violating effects. We can see that by considering antineutrinos, which transform between the two bases by complex conjugate of PMNS matrix and hence the imaginary term gets an opposite sign. It is also important to notice that from neutrino oscillations we can not measure neutrino masses directly, but only the differences of their squares. This leaves the absolute magnitude of neutrino masses undetermined and there are two possible mass orderings, the so called "normal hierarchy"  $m_1 < m_2 < m_3$  and "inverted hierarchy"  $m_3 < m_1 < m_2$ .

# 3.2 Experiments

Neutrinos are still not fully understood and pose an open question in today particle physics. The minimal standard model (SM) can not explain the origin of their masses in a renormalizable way and the parameters responsible for oscillations are known with rather poor precision compared

to the free parameters of the SM. There have been numerous neutrino experiments, many of which are still running today. They have all confirmed the existence of neutrino oscillations, however precision measurements of neutrinos are very hard because of their small masses and neutral electric charge.

Oscillations between all 3 flavors make determination of parameters fairly complicated, therefore most of the experiments focus on special cases, where only certain mass states are relevant. More precisely, experiments have shown that one mass difference is much smaller the the other two,  $\Delta m_{21}^2 \ll \Delta m_{31}^2 \approx \Delta m_{32}^2$ . Using this with (3.5), we see that it is sensible to consider the following two regimes, large and small L/E. In the first case oscillations mediated by the larger mass splitting average out. This is typically realized when observing neutrinos coming from the sun or low energy reactor neutrinos and is referred to as the solar neutrino oscillations. In the second case the oscillations mediated by the smaller mass splitting are negligible. This is a good approximation in for the atmospheric and accelerator neutrinos, as well as short baseline reactor neutrinos and is referred to as the atmospheric neutrino oscillations. This two regimes allow us to measure only a subset of the PMNS parameters and one mass splitting in a particular experiment, which makes the measurements much more precise.

#### 3.2.1 Solar and long baseline reactor experiments

As I already mentioned in the introduction, the first clue of neutrino oscillations came from solar experiments. One of the most successful ones is Super-Kamiokande in Japan, which uses 50,000 tons of highly pure water as a medium for elastic scattering  $\nu_e + e^- \rightarrow \nu_e + e^-$ . In this process electrons get accelerated to relativistic energies and emit Cherenkov radiation, which is then detected by scintillators. There are many other experiments, e.g. SNO and Borexino, which use the same principal and also experiments that utilize different detection methods, e.g. Gallex, which measured the rate of  $\nu_e + {}^{71}\text{Ga} \rightarrow {}^{71}\text{Ge} + e^+$  process. Same regime of neutrino oscillations can be also observed in reactor experiments, among which the most renowned is KamLAND in Japan.

Fusion processes in the sun produce a huge flux of  $v_e$ , which can be detected on Earth, despite the large distance. The main neutrino production

3.2 Experiments 17

processes are [7]

$$p + p \to {}^{2}\text{H} + e^{+} + \nu_{e}$$

$${}^{3}\text{He} + p \to {}^{4}\text{He} + e^{+} + \nu_{e}$$

$${}^{7}\text{Be} + e^{-} \to {}^{7}\text{Li} + \nu_{e}$$

$${}^{8}\text{B} \to {}^{7}\text{Be} + e^{+} + \nu_{e}$$

$${}^{13}\text{N} \to {}^{13}\text{C} + e^{+} + \nu_{e}$$

$${}^{15}\text{O} \to {}^{15}\text{N} + e^{+} + \nu_{e}$$
(3.6)

Nuclear reactors produce large amounts of  $\bar{\nu}_e$  through the fission processes  $_Z^A X \to _{Z+1}^A X + e^- + \bar{\nu}_e$  which can also be used for neutrino oscillation experiments. The energy of solar neutrinos reaches up to tens of MeV, therefore we can safely assume that the oscillations mediated by larger mass splitting average out. The same is true for long baseline reactor experiments, where typical neutrino energies are around 5 MeV and travel distances are around few hundred km, so the ratio E/L is still smaller then  $\Delta m_{31/32}^2$  ( $\Delta m_{31/32}^2$  is shorthand notation for when either  $\Delta m_{31}^2$  or  $\Delta m_{32}^2$  can be used). Using equation (3.5) along with the approximations

$$\langle \sin^2(\frac{\Delta m_{31/32}^2}{4E}L)\rangle = \frac{1}{2} \quad , \quad \langle \sin(\frac{\Delta m_{31/32}^2}{2E}L)\rangle = 0$$

we obtain the following survival probability for  $\nu_e$ :

$$P(\nu_e \to \nu_e) = 1 - \frac{1}{2} \sin^2(2\theta_{13}) + \cos^4\theta_{13} \sin^2(2\theta_{12}) \sin^2(\frac{\Delta m_{21}^2}{4E}L)$$
(3.7)

From here we can see that the full probability for solar oscillations depends only on two PMNS angles,  $\theta_{12}$  and  $\theta_{13}$ . By reconstructing the energy of incoming neutrinos and measuring their flux, the values of these parameters and mass splitting  $\Delta m_{21}^2$  can be determined. The expression (3.7) holds for neutrinos traveling through vacuum or a medium with negligible density. However, due to the high electron density inside the sun, neutrinos experience coherent forward scattering. This phenomenon is known as the Mikheev-Smirnov-Wolfenstein (MSW) effect and we need to take it into the account when observing solar neutrino oscillations. To describe the propagation of neutrinos in medium, we must consider the effective Hamiltonian and not the free one, as it was the case in vacuum. The interaction between neutrinos and electrons is described by Fermi theory (at

low energies, that we are interested in), with following Lagrangian

$$L_{eff} = -\frac{G_F}{\sqrt{2}} \bar{\nu}_e \gamma^{\mu} (1 - \gamma^5) e \cdot \bar{e} \gamma_{\mu} (1 - \gamma^5) \nu_e$$

$$= -2\sqrt{2} G_F \bar{\nu}_e \gamma^{\mu} e \cdot \bar{e} \gamma_{\mu} \nu_e$$

$$= -2G_F n_e \bar{\nu}_e \gamma^0 \nu_e$$
(3.8)

In the first step we used the fact that active neutrino are left-handed fermions, i.e.  $\frac{1}{2}(1-\gamma^5)\nu_e=\nu_e$ . In the second step we neglected electric charge currents (which is indeed a good approximation for non-relativistic matter) and averaged the electrons over the medium,  $\langle \bar{e}_l e_k \rangle = \frac{1}{4} \gamma_{lk}^0 n_e$ , where  $n_e$  is the average electron density. Using this result we can write down the effective potential that electrons feel, when propagating through medium

$$V_{eff}(L) = \sqrt{2}G_F n_e(L) \tag{3.9}$$

Here  $n_e$  depends on the traveled distance, since electron density is higher in the center of the sun and decreases towards surface. To describe the propagation of neutrinos in the medium, we need to add the potential term to the free Hamiltonian. For simplicity only 2 neutrino flavors will be considered, which can be justified by the fact that in first order approximation only  $\nu_e$  take part in the interactions and the other flavor can be thought as average of  $\nu_\mu$  and  $\nu_\tau$ . The effective Hamiltonian, written in flavor basis, then takes the following form

$$\mathbf{H}_{eff}(L) = \mathbf{U}\mathbf{H}_0\mathbf{U}^{\dagger} + \mathbf{V}(L)$$

$$\mathbf{H}_0 = \begin{pmatrix} m_1 & 0 \\ 0 & m_2 \end{pmatrix} , \quad \mathbf{V} = \begin{pmatrix} V_{eff}(L) & 0 \\ 0 & 0 \end{pmatrix}$$
 (3.10)

Knowing the effective Hamiltonian, we can now write down the Schrodinger equation for evolution of states and compute the new eigenvalues in mass eigenbasis, i.e. the effective masses

$$i\frac{\mathrm{d}}{\mathrm{d}t} \begin{pmatrix} v_1 \\ v_2 \end{pmatrix} = \mathbf{U}^{\dagger} i \frac{\mathrm{d}}{\mathrm{d}t} \begin{pmatrix} v_e \\ v_{\alpha} \end{pmatrix} = \mathbf{U}^{\dagger} \mathbf{H}_{eff}(L) \begin{pmatrix} v_e \\ v_{\alpha} \end{pmatrix}$$

$$\Rightarrow \tilde{m}_{1,2}^2(L) = \frac{1}{2} \left[ (m_1 + m_2 + V_{eff}(L)) + \sqrt{(V_{eff}(L) - \Delta \tilde{m}^2 \sin(2\theta))^2 + (\Delta \tilde{m}^2)^2 \cos^2(2\theta)} \right]$$
(3.11)

3.2 Experiments 19

Here  $\Delta \tilde{m}^2 = \tilde{m}_1^2 - \tilde{m}_2^2$  and  $\theta$  is the mixing angle that rotates the state between the flavor and mass basis. Now we can compute the new mixing angle  $\theta_{\tilde{m}}$ , which is the rotation between the new mass eigenbasis and flavor basis. This yields

$$\sin(2\theta_{\tilde{m}}) = \frac{\sin(2\theta)}{\sqrt{(V_{eff}/\Delta\tilde{m}^2 - \cos(2\theta))^2 + \sin^2(2\theta)}}$$
(3.13)

By analyzing (3.12) and (3.13) we can gain some intuition for neutrino oscillations in a medium. We immediately see that oscillations can not occur when  $\sin 2\theta = 0$ , since then also  $\sin 2\theta_{\tilde{m}} = 0$ , which is what we would naively expect. When  $V_{eff}=0$  the effective masses  $\tilde{m}_{1,2}=m_{1,2}$  and mixing angle  $\theta_{\tilde{m}} = \theta$  reduce back to vacuum case, as they should. However, if  $V_{eff} \to \infty$ , then  $\sin 2\theta_{\tilde{m}} \to 0$ , meaning that oscillations can not take place. Another interesting case is, when  $V_{eff}/\Delta \tilde{m}^2 = \cos 2\theta$  in which the mixing becomes maximal, i.e.  $\sin 2\theta_{\tilde{m}} = 1$ . This is an important result, since it implies that for any non-zero  $\theta$ , there exists a value of  $V_{eff}/\Delta \tilde{m}^2$  at which the oscillation probability equals 1 and is called the MSW resonance. The consequence of the MSW effect in solar oscillations is that a certain amount of  $\nu_e$  oscillates into other flavors already before they leave the surface of sun. Since  $V_{eff}$  depends on electron density and neutrino energy the exact analysis is rather complicated, but must be taken into account when analyzing solar neutrino oscillation. In the simplified case of two flavors the relevant oscillation probability becomes [8, 9]

$$P_{sun}(\nu_e \to \nu_e) \approx \begin{cases} 1 - \sin^2(2\theta_{12}) & E < \sim 100 keV \\ \sin^2 \theta_{12} & E > \sim 1 MeV \end{cases}$$
(3.14)

### 3.2.2 Atmospheric and accelerator experiments

Experiments with atmospheric and accelerator neutrinos fall into the second regime, described at the beginning of the section, where L/E is small. Atmospheric neutrinos are produced by cosmic rays, as they scatter in the atmosphere and create showers of new particles, which decay into stable particles, including neutrinos. The most important neutrino production processes are

$$\pi^{+} \to \mu^{+} + \nu_{\mu} \quad , \quad \pi^{-} \to \mu^{-} + \bar{\nu}_{\mu}$$
 $\mu^{+} \to e^{+} + \nu_{e} + \bar{\nu}_{\mu} \quad , \quad \mu^{-} \to e^{-} + \bar{\nu}_{e} + \nu_{\mu}$  (3.15)

Due to high energy of cosmic rays, the produced neutrinos typically also have high energies, which allows us to use the approximations in given in

equation (??). In accelerator experiments, the accelerators are tuned to produce highly pure  $\nu_{\mu}$  and  $\bar{\nu}_{\mu}$  beams, which are then measured in detectors several hundred kilometers away. Since the produced neutrino energies are high but well known, the distance between production point and the detector can be tuned to measure only the atmospheric oscillations. In this limit we use the following approximations

$$\frac{\Delta m_{21}^2}{4E}L \ll 1 \quad \Rightarrow \quad \sin^2(\frac{\Delta m_{21}^2}{4E}L) \approx 0 \tag{3.16}$$

Combining this with (3.5) we obtain the following probabilities for disappearance of the  $\nu_{\mu}$  and appearance of  $\nu_{\tau}$ 

$$P(\nu_{\mu} \to \nu_{\mu}) = 1 - \sin^{2}(2\theta_{obs}) \sin^{2}(\frac{\Delta m_{31/32}^{2}}{4E}L)$$

$$\sin \theta_{obs} = \cos \theta_{13} \sin \theta_{23}$$
(3.17)

$$P(\nu_{\mu} \to \nu_{\tau}) = \sin^2(2\theta_{23})\cos^4\theta_{13}\sin^2(\frac{\Delta m_{31/32}^2}{4E}L)$$
 (3.18)

The Super-Kamiokande experiment is one of the most successful atmospheric neutrino experiments up to this date. It measures the atmospheric  $\nu_e$  and  $\nu_u$  fluxes and besides that, is also able to reconstruct the energies and directions of the incoming neutrinos. An interesting result coming from this measurement is that the measured  $\nu_{\mu}$  flux exhibits zenith angle dependency. This is due to different travel lengths from the production point, where cosmic ray hit the atmosphere, to the detector as is schematically shown in Figure 3.1. On the other hand, no such effect was measured in the  $v_e$  flux, as can be seen in Figure 3.2. This leads to the conclusion, that atmospheric neutrinos oscillate mainly between  $\nu_{\mu}$  and  $\nu_{\tau}$  flavors, while mixing with the electron flavor is negligible. Another observation was, that  $\nu_{\mu}$  coming from the below (other side of the Earth) was roughly half of the one coming from above. Since the travel distance is about 10 km in the first case and 13 000 km in the second and knowing that atmospheric neutrinos mainly oscillate between the muon and tau flavor, we see that the mixing must be close to maximal, i.e.

$$\sin^2(2\theta_{23}) \approx 1 \quad \Rightarrow \quad \theta_{23} \approx 45^\circ$$
 (3.19)

The accelerator experiments provide a good crosscheck for this results. The energy of neutrinos produced in accelerators and their travel distance are well known and therefore they give us better information about the mass splitting  $\Delta m_{31}^2$ . Together, this experiments can be used to determine the values of  $\theta_{13}$ ,  $\theta_{23}$  and  $\Delta m_{31/32}^2$ .

3.2 Experiments 21

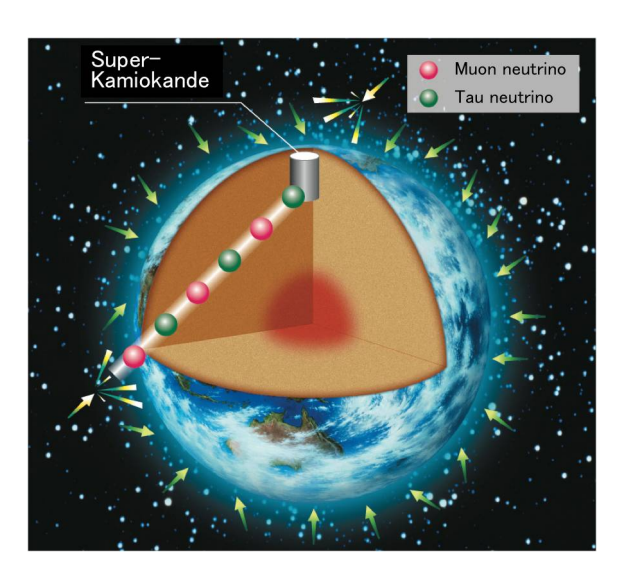


**Figure 3.1:** Schematic image showing the origin of angle dependency in the  $\nu_{\mu}$  flux in the Super-Kamiokande experiment.

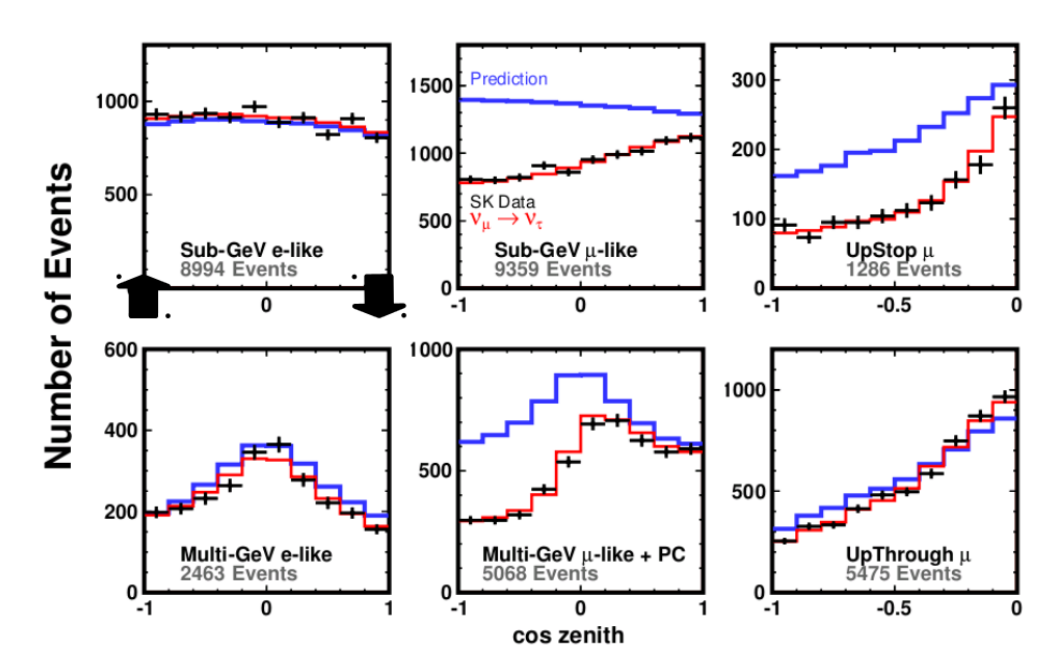


**Figure 3.2:** Measurement results from Super-Kamiokande [10] showing the zenith angle dependency of  $\nu_e$  and  $\nu_\mu$  fluxes. The predicted number of events in the absence of neutrino oscillations is marked with blue line, while the red line marks the predicted number of events when neutrino oscillations are included. The black dots are the measured data points.

#### 3.2.3 Short baseline reactor experiments

This is a special case of reactor experiments, where the detector is put much closer to the reactor, typically around 1 km. This allows us to neglect the solar oscillations mediated by the smaller mass splitting, since we are again in the small L/E regime, like in the atmospheric neutrino experiments. However, the probability for survival of  $\nu_e$  is much simpler then in the  $\nu_\mu$  case. Using equation (3.5) and approximation (3.16) we can derive

$$P(\nu_e \to \nu_e) = 1 - \sin^2(2\theta_{13})\sin^2(\frac{\Delta m_{31/32}^2}{4E}L)$$
 (3.20)

From this result we see, that the survival probability depends only on mixing angle  $\theta_{13}$  and mass splitting  $\Delta m_{31}^2$ . This  $\theta_{13}$  angle turns out to be very small, so short baseline reactor experiments are very important, since they measure it directly. The most successful among them are DayaBay in China, CHOOZ in France and RENO in South Korea. Their measurements concluded that  $\theta_{13}>0$  with more  $6\sigma$  then certainty [8] and added valuable data regarding the size of  $\Delta m_{31}^2$ . In Figure 3.3 the results from DayaBay experiment are presented, where the depth of the well can be related to the angle  $\theta_{13}$  and its broadness to  $\Delta m_{31/32}^2$ .

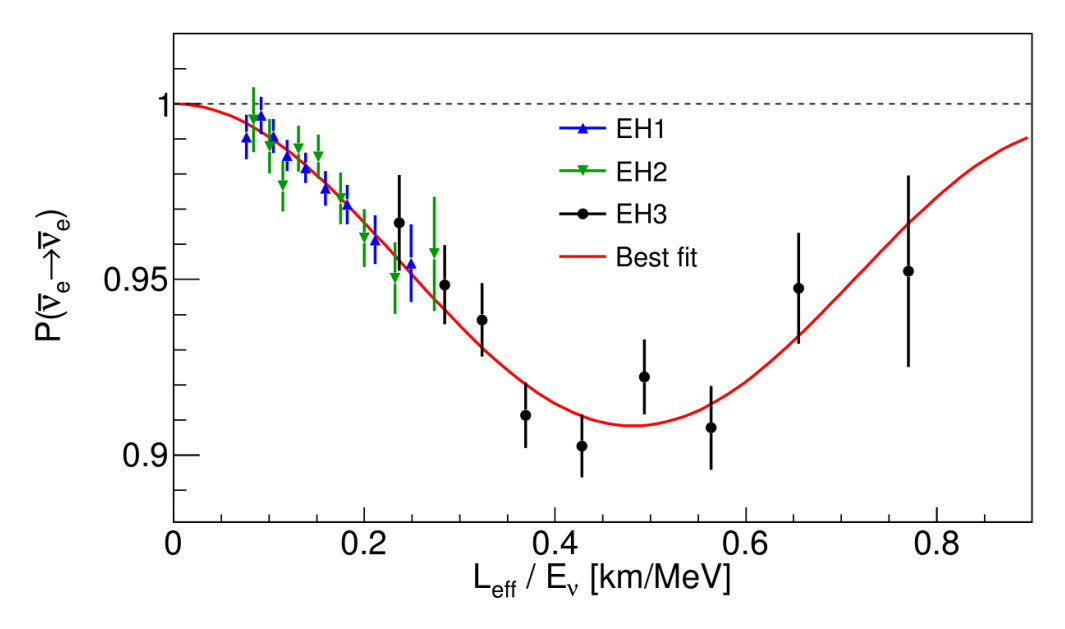


**Figure 3.3:** Measurement results for from DayaBay experiment [11], showing the  $\bar{\nu}_e$  disappearance probability. The red line shows the best fit theoretical prediction, while the data points come from detectors placed at different distances from the reactor.

# 3.3 Bounds on neutrino oscillation parameters

In the previous sections I discussed the theoretical background of neutrino oscillations and reviewed the most important experiments. From there we can see, that neutrino oscillation experiments can be used to determine the values of the PMNS matrix parameters ( $\theta_{12}$ ,  $\theta_{13}$ ,  $\theta_{23}$  and  $\delta_{CP}$ ) and the neutrino mass splittings ( $\Delta m_{21}^2$  and  $\Delta m_{31}^2$ ). However, since the oscillation parameters are intertwined in different experiments, we need somewhat more advanced statistical tools in order to correctly interpret the results. Most commonly the Chi-square ( $\chi^2$ ) test is used, which described in greater detail in the Appendix A. Its purpose is to characterize the probability, how well does a certain theoretical prediction fit the observations. In what follows, I will sum up the oscillation parameter bounds given by the NuFIT project, which are based on the latest experimental data available in summer 2014.

#### 3.3.1 NuFIT results

The NuFIT Collaboration [8] provides global analysis of neutrino oscillation measurements determining the leptonic mixing matrix and the neutrino masses in the framework of the Standard Model with 3 massive neutrinos. It is based on combination of different experiments, listed in [9], that cover both, solar and atmospheric oscillation regimes. The NuFIT results include the global best fit of the oscillation parameters, as well as one and two parameter projections of  $\Delta \chi^2$ . The best fit values for the oscillation parameters are collected in Table 3.1. One parameter and two parameter projections of  $\Delta \chi^2$  are displayed in Figure 3.4 and Figure 3.5 correspondingly. Based on these neutrino oscillation parameters constraints we can deduce the constraints on sterile-active neutrino mixing angles, as was already discussed in Section 2.3.

	Normal Ordering ( $\Delta \chi^2 = 0.97$ )		Inverted Ordering (best ft)		Any Ordering
	bfp ±1σ	3σ range	bfp ±1σ	3σ range	3σ range
$\sin^2 \theta_{12}$	$0.304^{+0.013}_{-0.012}$	0.270 → 0.344	$0.304^{+0.013}_{-0.012}$	0.270 → 0.344	0.270 → 0.344
$ heta_{12}$ / $^{\circ}$	33.48 <sup>+ 0.78</sup> <sub>- 0.75</sub>	31.29 → 35.91	33.48 <sup>+0.78</sup> <sub>-0.75</sub>	31.29 → 35.91	31.29 → 35.91
$\sin^2 \theta_{23}$	$0.452^{+0.052}_{-0.028}$	$0.382 \rightarrow 0.643$	$0.579^{+0.025}_{-0.037}$	0.389 → 0.644	0.385 → 0.644
$\theta_{23}$ / $^{\circ}$	42.3+3.0	38.2 → 53.3	49.5+1.5	38.6 → 53.3	38.3 → 53.3
$\sin^2 \theta_{13}$	0.0218+0.0010	0.0186 → 0.0250	$0.0219^{+0.0011}_{-0.0010}$	0.0188 → 0.0251	0.0188 → 0.0251
$\theta_{13}$ / $^{\circ}$	8.50+0.20	7.85 → 9.10	8.51+0.20	7.87 → 9.11	7.87 → 9.11
$\delta_{CP}/^{\circ}$	306+39	0 → 360	254 <sup>+63</sup> <sub>-62</sub>	0 → 360	0 → 360
$\frac{\Deltam_{21}^2}{10^{-5}\text{eV}^2}$	7.50+0.19	7.02 → 8.09	7.50+0.19	7.02 → 8.09	7.02 → 8.09
$\frac{\Delta  m_3^2}{10^{-3}   \text{eV}^2}$	+2.457+0.047	+2.317 → +2.607	$-2.449^{+0.048}_{-0.047}$	-2.590 → -2.307	+2.325 → +2.599 -2.590 → -2.307

**Table 3.1:** Three-flavor oscillation parameters fit to global data after the NOW 2014 conference. The numbers in the 1st (2nd) column are obtained assuming NO (IO), i.e., relative to the respective local minimum, whereas in the 3rd column we minimize also with respect to the ordering. Note that as atmospheric mass-squared splitting we use  $\Delta m_{31}^2$  for NO and  $\Delta m_{32}^2$  for IO.

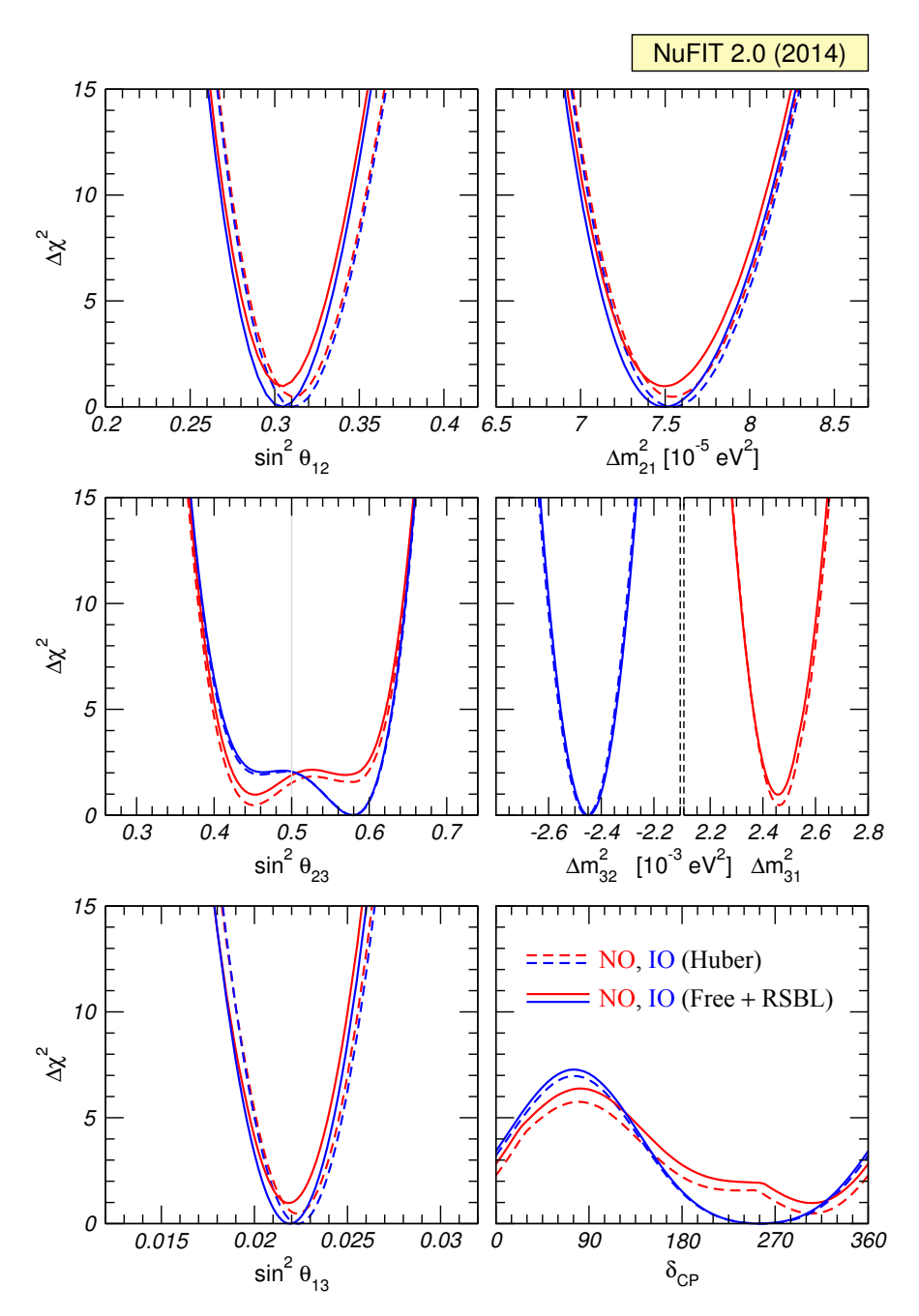


**Figure 3.4:** Global  $3\nu$  oscillation analysis. The red (blue) curves are for Normal (Inverted) Ordering. For solid curves the normalization of reactor fluxes is left free and data from short-baseline (less than 100 m) reactor experiments are included. For dashed curves short-baseline data are not included. Note that as atmospheric mass-squared splitting we use  $\Delta m_{31}^2$  for NO and  $\Delta m_{32}^2$  for IO.

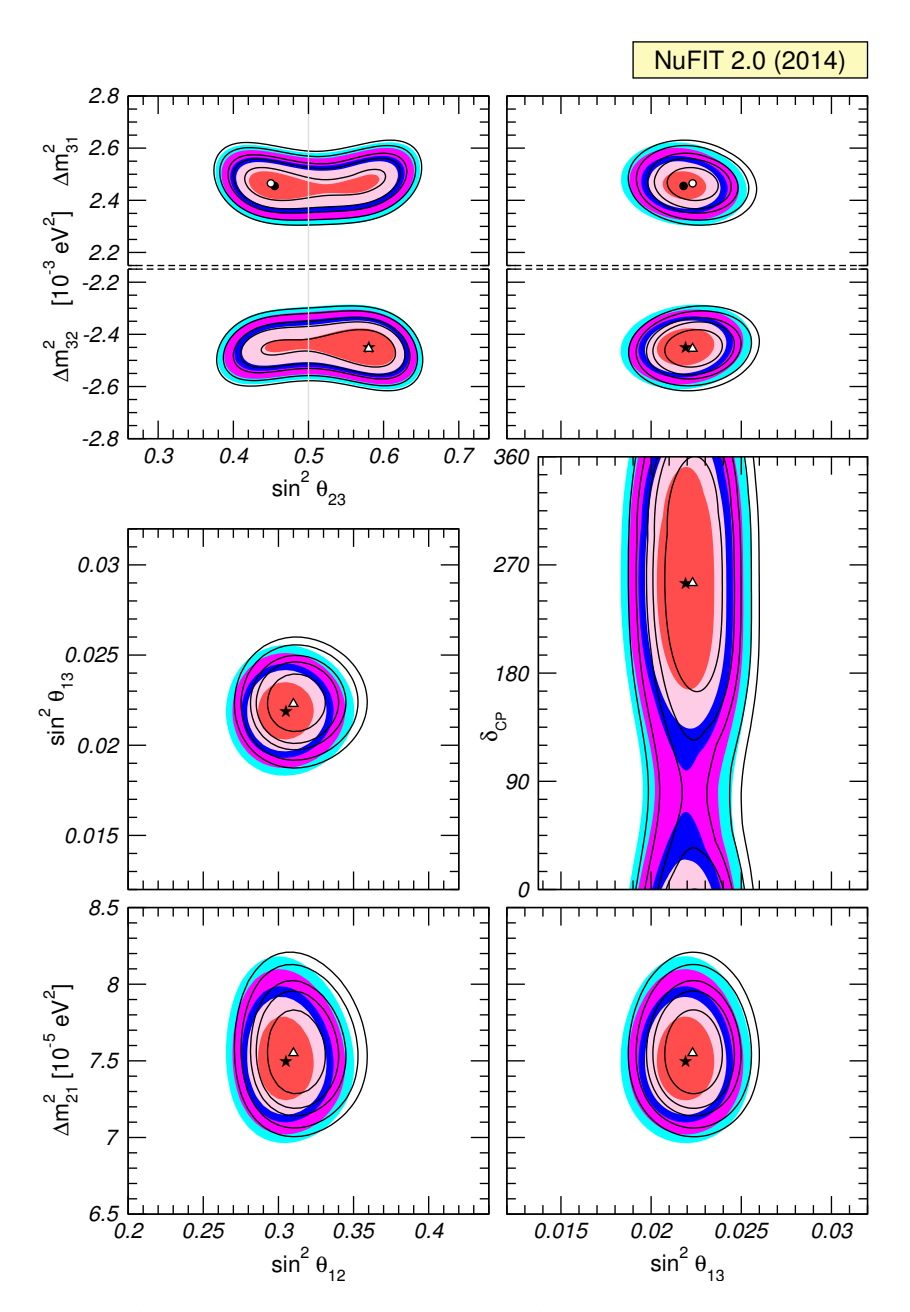


**Figure 3.5:** Global  $3\nu$  oscillation analysis. Each panel shows a two-dimensional projection of the allowed six-dimensional region after minimization with respect to the undisplayed parameters. The different contours correspond to  $1\sigma$ , 90%,  $2\sigma$ , 99% and  $3\sigma$  confidence level (at 2 degrees of freedom). Full regions correspond to the analysis with free normalization of reactor fluxes and data from short-baseline (less than 100m) reactor experiments included. For void regions short-baseline reactor data are not included. Note that as atmospheric mass-squared splitting we use  $\Delta m_{31}^2$  for NO and  $\Delta m_{32}^2$  for IO.

# 3.4 Bounds on sterile-active neutrino mixing angles

In the previous chapter, Section 2.3, it was shown that the mixing angles between sterile and active neutrinos depend on free parameters  $M_N$  and z. Therefore, it is more sensible to consider the mixing angle ratios, (2.17) and (2.18), as the do not depend on these two parameters. However, also the mixing angle ratios can not be uniquely determined, due to Majorana phases and uncertainties regarding the neutrino oscillation parameters. Therefore it is common to find their minimum and maximum possible values at some chosen confidence level. For this purpose I wrote a computer program that scanned over the all possible values of oscillation parameters, within their  $3\sigma$  intervals, and Majorana phases. The analysis was performed in two different ways, first neglecting the correlation between oscillation parameters and second including the pairwise correlations of the parameters. The latter provide additional information which is lost when considering only  $\Delta \chi^2$  likelihood of single parameters. For this reason the bounds on mixing angle ratios coming from the correlated analysis are expected to be stronger.

#### 3.4.1 Evaluation

As already mentioned, the values of mixing angle ratios  $T_{\alpha}$  were obtained using a custom computer program. The essence of the algorithm is the evaluation of (2.17) and (2.18) in nested for-loops, where each of them runs over allowed interval for one of the parameters. In this way one can obtain the values of the mixing angle ratios over the whole parameter space, however such algorithm doesn't account for the correlations between parameters. In order to include the correlation information, the allowed ranges for parameters in sub-loops need to be readjusted at every step, since they depend on the values of the fixed parameters from higher level loops.

As discussed in Section 3.2 there are different types of neutrino oscillation experiments, which gives us information about different oscillation parameters. It was shown that (under the discussed approximations) the (dis)appearance probability of active neutrinos always depends on mixing angle  $\theta_{13}$ , which can also be measured independent of other parameters in short baseline experiments. The mixing angle  $\theta_{12}$  and mass difference  $\Delta m_{21}^2$  can be obtained from solar and long baseline experiments and are correlated with each-other, as well as with  $\theta_{13}$ . Similarly,  $\theta_{23}$  and

 $\Delta m_{31/32}^2$ , measured by atmospheric and accelerator experiments, are also correlated with each-other and  $\theta_{13}$ . Based on this consideration we can construct an algorithm that correctly accounts for the correlations of different parameters in the following way. First we take the  $\theta_{13}$  range at chosen certainty level and start iterating over it. For each value of  $\theta_{13}$ we can obtain the allowed intervals of  $\theta_{12}$  and  $\theta_{23}$  from the correlated data and run the iterations over them (the order doesn't matter, since  $\theta_{12}$  and  $\theta_{23}$  are uncorrelated). More precisely, the allowed intervals are  $\{\theta_{12/23} : \Delta \chi^2(\theta_{13}, \theta_{12/23}) < \Lambda\}$ , where  $\Lambda$  is the value of the  $\chi^2$  distribution at the confidence level we are interested in. In each step of iteration over  $\theta_{12}$  we then determine the allowed intervals for  $\Delta m_{21}^2$  at current values  $\theta_{13}$  and  $\theta_{12}$  and similarly allowed intervals for  $\Delta m_{31/32}^2$  at current  $\theta_{13}$  and  $\theta_{23}$ . We could first determine the allowed mass difference intervals at certain  $\theta_{13}$  and then look at allowed ranges of  $\theta_{12}$  and  $\theta_{23}$ , however the result would be the same. This is because the third level intervals are simply a cross section of the intervals given by pairwise correlations with higher level parameters. To be concrete, the range for  $\Delta m_{21}^2$  is  $\{\Delta m_{21}^2 : \Delta \chi^2(\theta_{13}, \Delta m_{21}^2) < \Lambda\} \cap \{\Delta m_{21}^2 : \Delta \chi^2(\theta_{12}, \Delta m_{21}^2) < \Lambda\}$ , which applies analogously to  $\Delta m_{31/32}^2$ , correlated with  $\theta_{23}$  instead of  $\theta_{12}$ . This ranges have at least the confidence level of  $\Delta \chi^2 = \Lambda$  or higher, since they are deduced from pairwise correlations. An interval corresponding strictly to chosen confidence level could only be determined by using information of higher order correlation; in case of  $\Delta m_{21}^2$  that would be  $\{\Delta m_{21}^2 : \Delta \chi^2(\theta_{13}, \theta_{12}, \Delta m_{21}^2) < \Lambda\}$ , however such information was not available. Finally the  $\Delta m_{21}^2$  and  $\Delta m_{31/32}^2$  intervals are evaluated over, along with the  $\delta_{CP}$  and Majorana phases. At each step of evaluation the mixing angle ratios are stored, if they exceed (are below) the previous maximum (minimum) value, along with the corresponding parameters

#### 3.4.2 Results

The computations were run using the neutrino oscillation parameters and their correlations published in [8]. For consistency, I compare the results with the ones published in [12]. The obtained mixing angle ratios are presented in Table 3.2. From there we can see that the new oscillation data puts somewhat stronger constrains on the mixing angle ratios. Difference is the biggest for the electron flavor, where the upper bound is pushed down by roughly 3% in case of NH and 2,5% in case of IH. This is due to much preciser measurement of the  $\theta_{13}$  in DayaBay experiment, complemented by RENO and Double Chooz data. On the other hand, the

differences in muon and tau flavor are all less then 1%. From the comparison of uncorrelated and correlated analysis we see that the differences are negligible. The reason for this is, that the uncertainties on oscillation parameters have much smaller effect on the mixing angle ratios then the unconstrained Majorana phases  $\zeta$  and  $\xi$ . This can be seen from Equations (2.17) and (2.17), where particular values of  $\zeta$  and  $\xi$  lead to cancellation of the two terms within the absolute value squared, resulting in minimal  $T_{\alpha}$ , while at other values the same terms will add up, giving maximal  $T_{\alpha}$ .

Ratio	2011 Data	NuFIT uncorrelated	NuFIT correlated
$T_e^{NH}$	0 - 0.17	0.00(2) - 0.14	0.00(3) - 0.14
$T_{\mu}^{NH}$	0.07 - 0.92	0.08 - 0.91	0.08 - 0.91
$T_{ au}^{NH}$	0.06 - 0.90	0.06 - 0.90	0.07 - 0.89
$T_e^{IH}$	0.02 - 0.98	0.02 - 0.96	0.02 - 0.96
$T_{\mu}^{IH}$	0 - 0.63	0 - 0.62	0 - 0.62
$T_{ au}^{IH}$	0 - 0.65	0 - 0.65	0 - 0.65

**Table 3.2:** Table with obtained sterile-active neutrino mixing angle ratios, defined in (2.14), at  $3\sigma$  confidence level. In the first column there are the results from [12] obtained with older (2011) constraints on neutrino oscillation parameters. In the second column are the uncorrelated results and in third the column the correlated results, obtained with the NuFIT data [8]. The superscript NH and IH denote normal and inverted hierarchy respectively.

As shown before, the values of the sterile-active neutrino mixing angles can be easily obtained from the mixing angle ratios. Their values, calculated for  $M_N=1$  GeV and |z|=10, are presented in Table 3.3. This results can be simply generalized for other values of  $M_N$  and  $|z|^2\gg 1$ , since  $\vartheta_{\alpha} \propto \frac{|z|^2}{M_S}$ .

Flavor	minimum	maximum
$\vartheta_e^{NO}$	$1.3 \times 10^{-11}$	$6.1 \times 10^{-10}$
$artheta_{\mu}^{NO}$	$3.8 \times 10^{-10}$	$4.2 \times 10^{-9}$
$artheta^{NO}_{ au}$	$3.2 \times 10^{-10}$	$4.1 \times 10^{-9}$
$\vartheta_e^{IO}$	$1.6 \times 10^{-10}$	$7.7 \times 10^{-9}$
$artheta_{\mu}^{IO}$	0	$4.9 \times 10^{-9}$
$artheta^{IO}_{ au}$	0	$5.2 \times 10^{-9}$

**Table 3.3:** Table with obtained sterile-active neutrino mixing angles for  $M_S = 1$ GeV and |z| = 10, calculated from the mixing angle ratios (based on correlated data) presented in Table 3.2. The superscripts NH and IH denote normal and inverted hierarchy correspondingly.



# Direct detection searches

As already discussed in the previous chapters there is strong theoretical motivation to assume the existence of sterile neutrinos. This led to numerous experimental searches in wide mass ranges, spanning from as low as eV up to few GeV. The strongest and most reliable constraints come from direct detection experiments in accelerators. No event associated with sterile neutrino was ever detected, which gives us an upper bound on sterile-active neutrino mixing angles defined in (2.9). A thorough review of different possible experiments and their sensitivity can be found in [13]. The main constrains come from fixed target experiments, while the constraints from other measurements are weaker. These can be either peak searches or beam dump experiments, which both study meson decays and were used to establish upper bounds on the mixing angles for sterile neutrinos in mass range from few tens of MeV up to approximately 2 GeV.

In the following Section 4.1 the peak search experiments are presented along with the strongest constraints on sterile-active neutrino mixing angles of this type. That is followed by Section 4.2 which discusses the direct detection experiments. The bounds coming this kind of experiments are not universal and some of them need reinterpretation for the case of considered model. Finally, the direct detection experiment bounds are combined with the constraints coming from neutrino oscillations, derived in 3.3, to obtain the lower limits on sterile neutrino lifetimes.

## 4.1 Peak search experiments

In peak search experiments leptonic two body decays of  $\pi^+$  or/and  $K^+$  mesons are studied. The mesons are produced by hitting a high intensity proton beam into production target and subsequently separated from other particles using magnetic field. After that they decay and the produced daughter particles are observed. Particularly interesting are the two body decays, since the energies of the daughter particles take fixed values (delta peaks in the energy spectrum), determined solely by energy and momentum conservation. This allows for searches of sterile neutrinos, since they should produce a secondary peak in the charged lepton energy spectrum, besides the primary peak associated with the decays into charged lepton and corresponding active neutrino. No suitable events were ever detected, which puts an upper bound on the active-sterile neutrino mixing angle. An advantage of peak search experiments is that their analysis is based purely on kinematics and therefore model independent [14], as long as the searched particles are produced in such decays.

In  $\pi$  decays the primary peak comes from  $\pi^+ \to e^+ \nu_e$  decay, while the secondary peak coming from  $\pi^+ \to e^+ N$  decay is searched for. Most recent experiment of this type was preformed by PIENU Collaboration [15] for sterile neutrinos in the mass range 60 - 129 MeV, which puts an upper bound on  $\vartheta_e^2$  at level of  $10^{-8}$ . Older results for the mass range 50 - 130 MeV can be found in [16], which contains also bounds for smaller masses (4 MeV - 60 MeV) based on the deviation of the number of events in the primary positron peak from the predicted SM value. Similar experiments with charged K mesons were recently preformed by E949 Collaboration [17] and previously by KEK [18, 19], obtaining upper bounds on  $\vartheta_e^2$  and  $\vartheta_\mu^2$  up to sterile neutrino masses of 340 MeV. The summary of the experimental bounds on  $\vartheta_e^2$  and  $\vartheta_\mu^2$  is presented in Figure 4.1 and 4.2.

# 4.2 Beam dump experiments

This type of experiment relies on high energy proton beam which is dumped on a solid target producing large amount of daughter particles. Vast majority of them is stopped by absorber and only neutrinos which originate from prompt meson decays penetrate through. After the absorber is the decay chamber in which candidate events for sterile neutrino decay are searched for. The probability for such an event is proportional to the product of branching ratio for meson's leptonic and semileptonic decays into sterile neutrino  $Br(X \to l_{\alpha}N...) \propto \vartheta_{\alpha}^2$  and sterile neutrino's

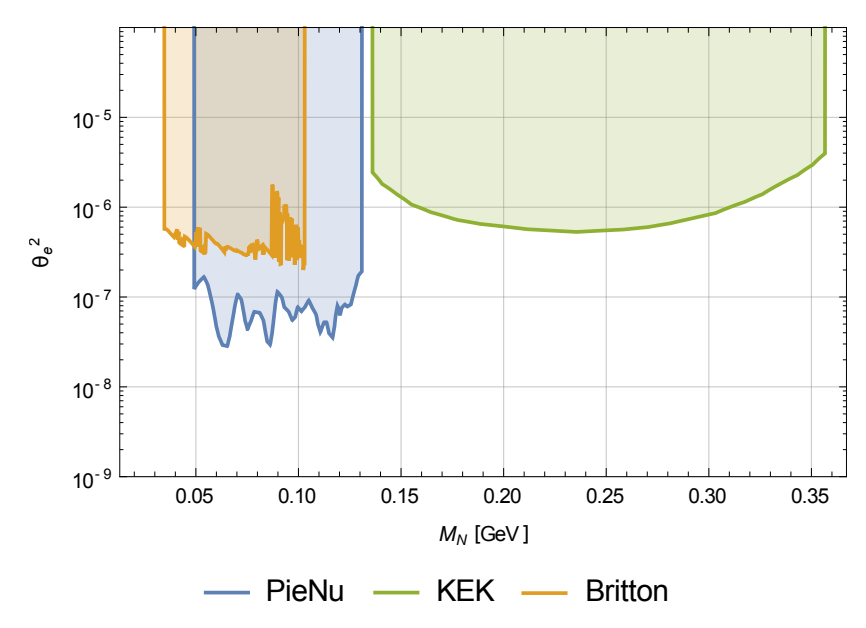


**Figure 4.1:** Value of the sterile-active neutrino mixing angle  $\theta_e^2$  as a function of the sterile neutrino mass  $M_N$ , based on PieNu [15], KEK [17] and Britton et. al. [16] data.

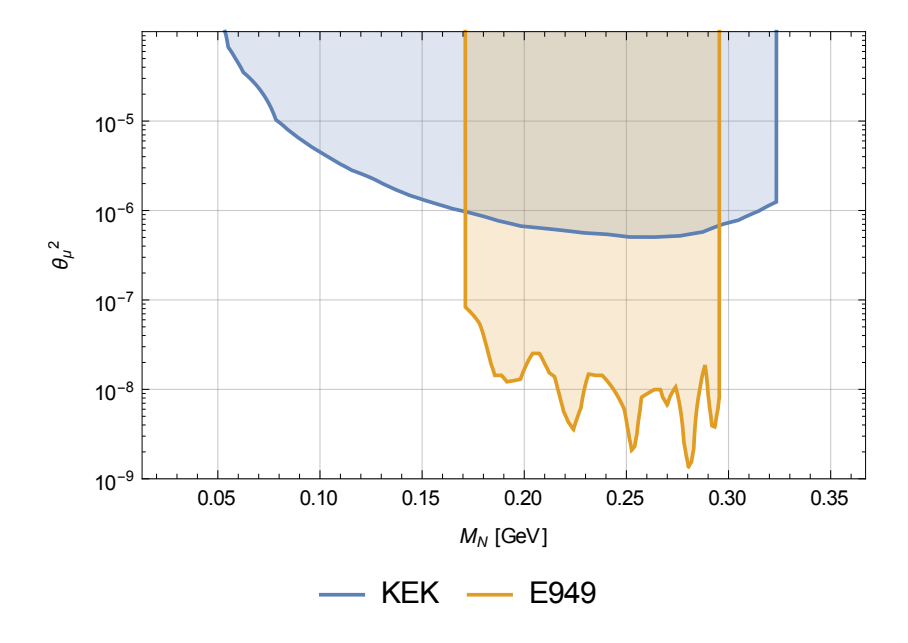


**Figure 4.2:** Value of the sterile-active neutrino mixing angle  $\vartheta_{\mu}^2$  as a function of the sterile neutrino mass  $M_N$ , based on KEK [18] and E949 Collaboration [17] data.

branching ratio for the observed decay channels  $Br(N \to \nu_{\beta} l_{\beta}...) \propto \vartheta_{\beta}^2$ . Therefore the signal is proportional to  $\vartheta_{\alpha}^2 \vartheta_{\beta}^2$  and not just  $\vartheta_{\alpha}^2$  as in peak search experiments. The bounds from this type of experiments are however model dependent, since the heavy neutrino branching ratios may differ in various models.

Strongest constraints for sterile neutrino masses  $M_N \leq 400$  MeV come from CERN PS191 experiment [20, 21], where signatures of  $\pi$  and K decays through heavy neutral lepton were searched for. It is important to note that in the original analysis heavy neutrinos were assumed to interact only through charge-current (CC) processes mediated by  $W^{\pm}$  bosons, while in case of  $\nu MSM$  Lagrangian (2.3) also neutral-current (NC) interactions mediated by Z bosons are possible. This was already pointed out in [12, 28], where similar analyses were preformed. Consequently the upper bounds on mixing angles are stronger, since the expected number of events is higher due to additional NC decay channels. The original limits on neutrino mixing angles  $|U_{eI}|^2$  that come from  $\pi^+/K^+ \to e^+N \to$  $e^+(\nu_e e^+ e^- + c.c)$  decays did not take into account the  $N \to \nu_\alpha e^+ e^- + c.c.$ decays, where  $\alpha = \mu$ ,  $\tau$ . From the comparison of the assumed and actual decay widths, given by Equations (B.17) and (B.18), we can see that the mixing angle from the original interpretation  $|U_{eI}|^2$  puts an upper bound on the following combination of the mixing angles  $\vartheta_{\alpha}$ 

$$|U_{eI}|^4 \ge \vartheta_e^2 (C_3 \vartheta_e^2 + C_1 (\vartheta_u^2 + \vartheta_\tau^2)) \tag{4.1}$$

where  $C_1$  and  $C_3$  are constants related to the Weinberg angle. Similarly, the limits on  $|U_{eI}U_{\mu I}|$  coming from  $\pi^+/K^+ \to \mu^+ N \to \mu^+(\nu_e e^+ e^- + c.c.)$  did not include the  $N \to \nu_\alpha e^+ e^- + c.c.$  decays, which gives us the following relation \*

$$|U_{\mu I}U_{eI}|^2 \ge \vartheta_{\mu}^2(C_3\vartheta_e^2 + C_1(\vartheta_{\mu}^2 + \vartheta_{\tau}^2))$$
(4.2)

The bounds  $|U_{eI}|^2$  and  $|U_{eI}U_{\mu I}|$  coming from  $K^+ \to e^+ N \to e^+ (e^- \pi^+ + c.c)$  and  $K^+ \to e^+ N \to e^+ (\mu^- \pi^+ + c.c)$  however are possible only through CC and therefore need no reinterpretation. Same is true for bounds on  $|U_{\mu I}|^2$ , which are based on  $K^+ \to \mu^+ N \to \mu^+ (\mu^- e^+ \nu_e + c.c.)$  and  $K^+ \to \mu^+ N \to \mu^+ (\mu^- \pi^+ + c.c.)$  decays. The rescaling relations (4.1) and (4.2) do not fix the the upper bounds on mixing angles  $\vartheta_\alpha$  uniquely, however using the mixing angle ratios mediated by neutrino oscillations one can find a

<sup>\*</sup>Here I must add, that it is not perfectly clear, how the different decay channels, which have the same final states, could have been distinguished. However, assuming this can be done, as is apparent from [21] data, the preformed analysis provides the most accurate reinterpretation of the bounds.

lower bound on lifetime  $\tau$  of sterile neutrinos. It is inversely proportional to the total decay width  $\Gamma_{total}$ , which is a linear combination of  $\vartheta_{\alpha}^2$  with corresponding mass dependent prefactors  $f_{\alpha}(M_N)$  (see Appendix B)

$$\tau = \frac{\hbar}{\Gamma_{total}} \propto \frac{1}{\sum_{\alpha} f_{\alpha}(M_N) \,\vartheta_{\alpha}^2} \tag{4.3}$$

In order to obtain the minimal lifetime the  $\vartheta_{\alpha}$  were varied within their allowed  $3\sigma$  ranges, obeying the constraints from neutrino oscillations data and direct detection experiments. The resulting lifetimes for original interpretation and the considered model are presented in Figure 4.3, where we can see that in case of NH the bound gets an order of magnitude stronger, while for IH it remains unchanged.

Further bounds on mixing angles of heavy neutrino in the mass range 10 MeV - 1.5 GeV come from CHARM Collaboration [22, 23]. Similarly to the PS191 Collaboration, they searched for D meson decays into heavy neutrinos and their subsequent decays into leptons. Again only CC interactions were considered, therefore the bounds had to be rescaled similarly as in the case of PS191 experiment. However, CHARM experiment studied decays of D mesons, which have much higher mass then pions and kaons, therefore additional decay channels for sterile neutrinos, discussed in Appendix B.1.1 and B.1.2, had to be included into the rescaling. The bounds can be additionally strengthened by more accurate computation of N production in D meson decays. The original analysis estimated its rate based on the branching ratio of pure leptonic decays,  $Br(D^+ \to l_\alpha^+ N)$ . Such decays are significant only for heavy neutrinos and become helicity suppressed as  $M_N \to 0$  (which is also the case in when  $\nu_\alpha$  is produced instead of N). Therefore at  $M_N \leq 0.7$  GeV semi-leptonic decays, e.g.  $D^+ \to \bar{K}^0 e^+ N$ , become the main source of sterile neutrinos. Additionally, in the original publication the upper bounds on  $|U_{eI}|^2$  and  $|U_{uI}|^2$  were obtained by assuming that both processes in decay chain were proportional to the same mixing angle. We can obtain stronger bounds by taking into the account that sterile neutrinos can be produced through mixing with an active neutrino of any flavor. As a consequence the mixing angles can not be uniquely fixed, however using the constraints from neutrino oscillations we can minimize the lifetime of sterile neutrinos, as discussed before. The original and reinterpreted analysis of CHARM data is show in Figure 4.4. We can see that the updated bounds form CHARM experiment become significantly stronger, however it turns out to be important only for normal hierarchy, since the bounds from NuTeV [24] are stronger in the inverted case.

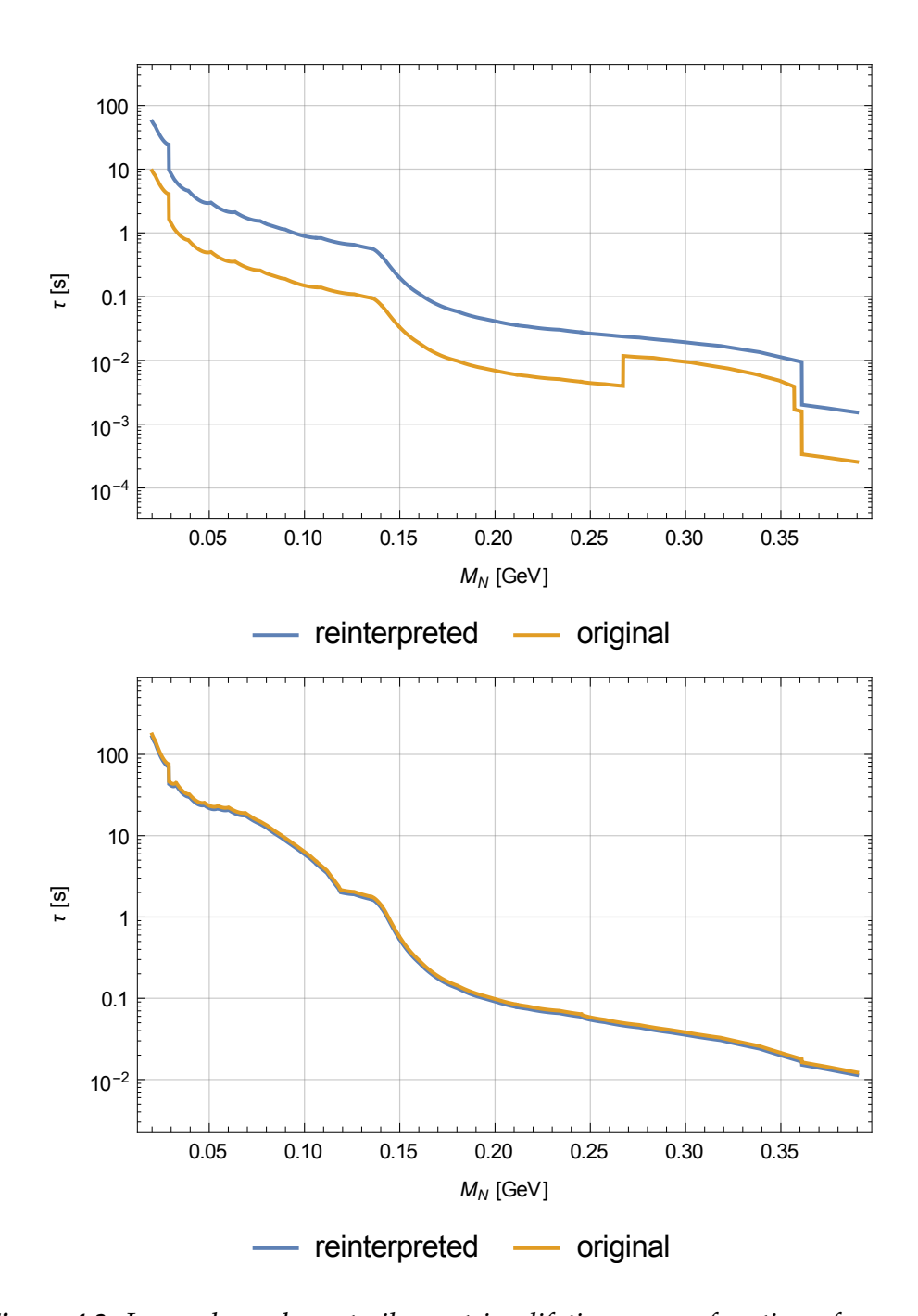


**Figure 4.3:** Lower bound on sterile neutrino lifetime  $\tau$  as a function of mass its  $M_N$  coming from the PS191 experiment. The blue line and yellow line were obtained using the original and reinterpreted mixing angles correspondingly. The upper plot is for the case of normal hierarchy and the bottom one for inverted hierarchy.

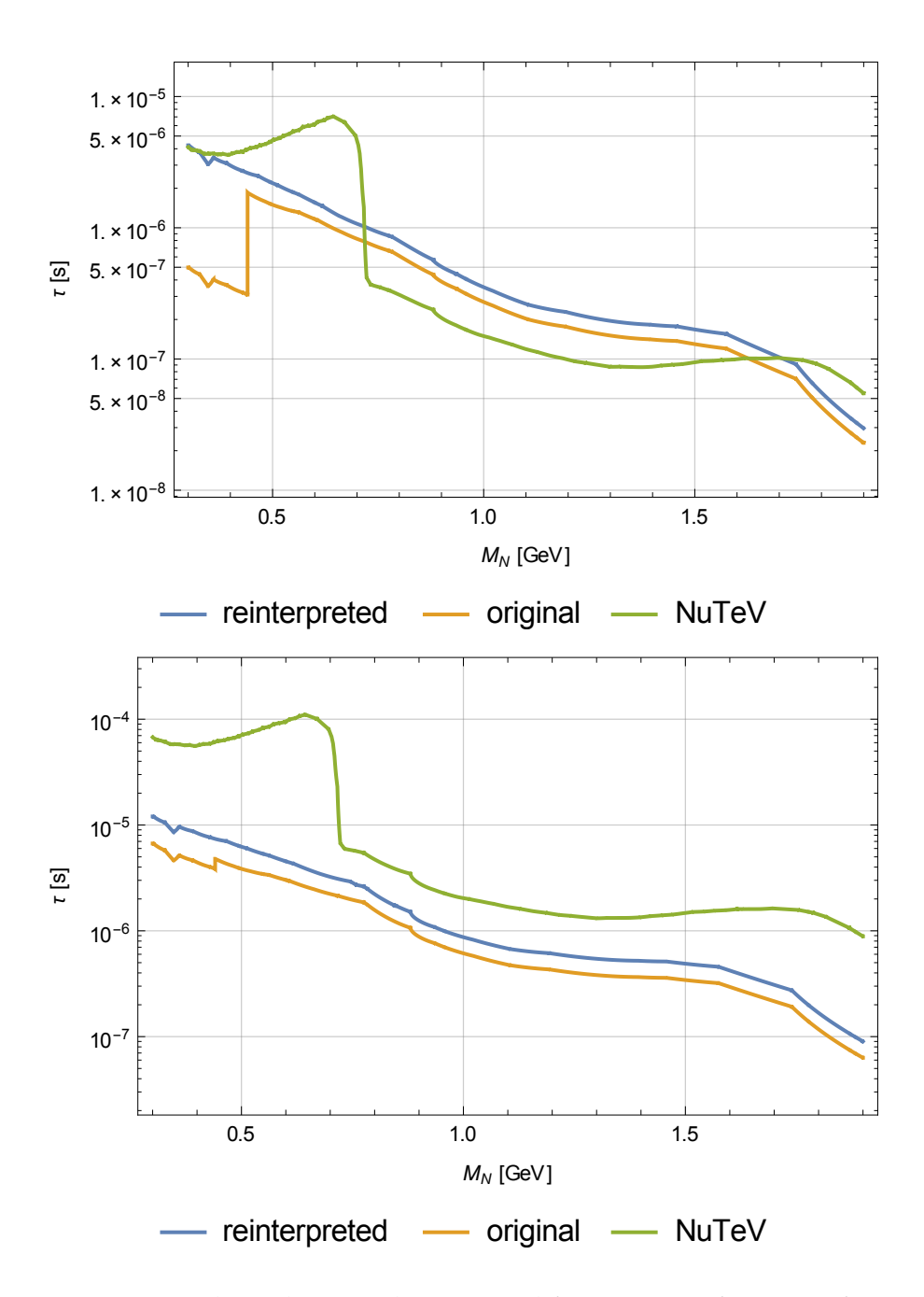


**Figure 4.4:** Lower bound on sterile neutrino lifetime  $\tau$  as a function of mass its  $M_N$ . The blue line and yellow line were obtained using the original and reinterpreted CHARM data [23], while green is based on NuTeV experiment [24]. The upper plot is for the case of normal hierarchy and the bottom one for inverted hierarchy.

### 4.3 Combined direct detection bounds

Combination of neutrino oscillation constraints and direct detection bounds, coming from peak searches and beam dump experiments were used to infer global lower bounds on sterile neutrino lifetimes. The results obtained with original and reinterpreted measurements are presented in Figure 4.5. The corresponding mixing angles, varied in the allowed ranges so that they minimize the lifetime, from all the considered experiments are presented in Figure 4.6 for normal and Figure 4.7 for inverted hierarchy.

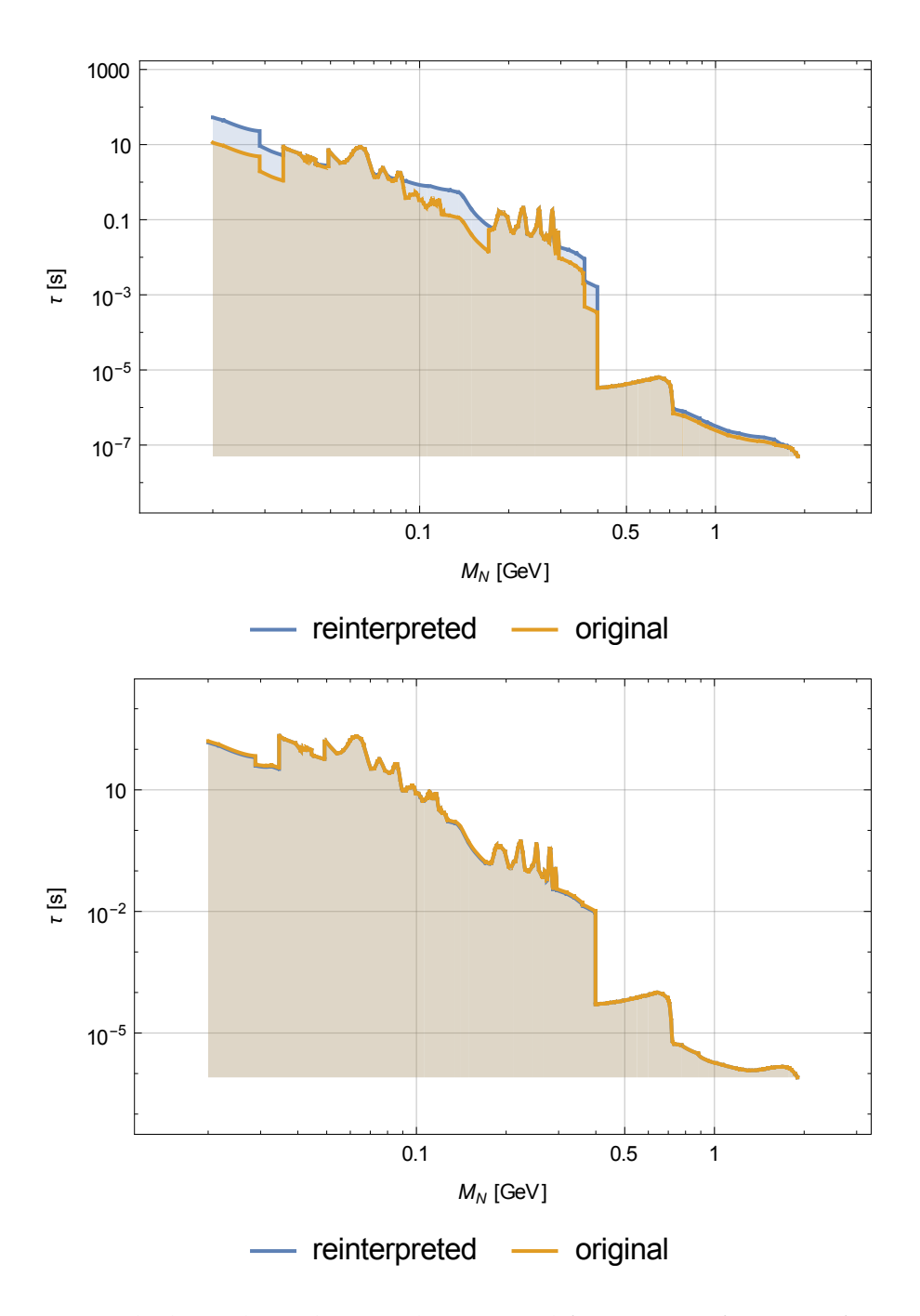


**Figure 4.5:** The lower bound on sterile neutrino lifetime  $\tau$  as a function of mass its  $M_N$ . The blue line and yellow line were obtained using the original and reinterpreted data correspondingly. The upper plot is for the case of normal hierarchy and the bottom one for inverted hierarchy.

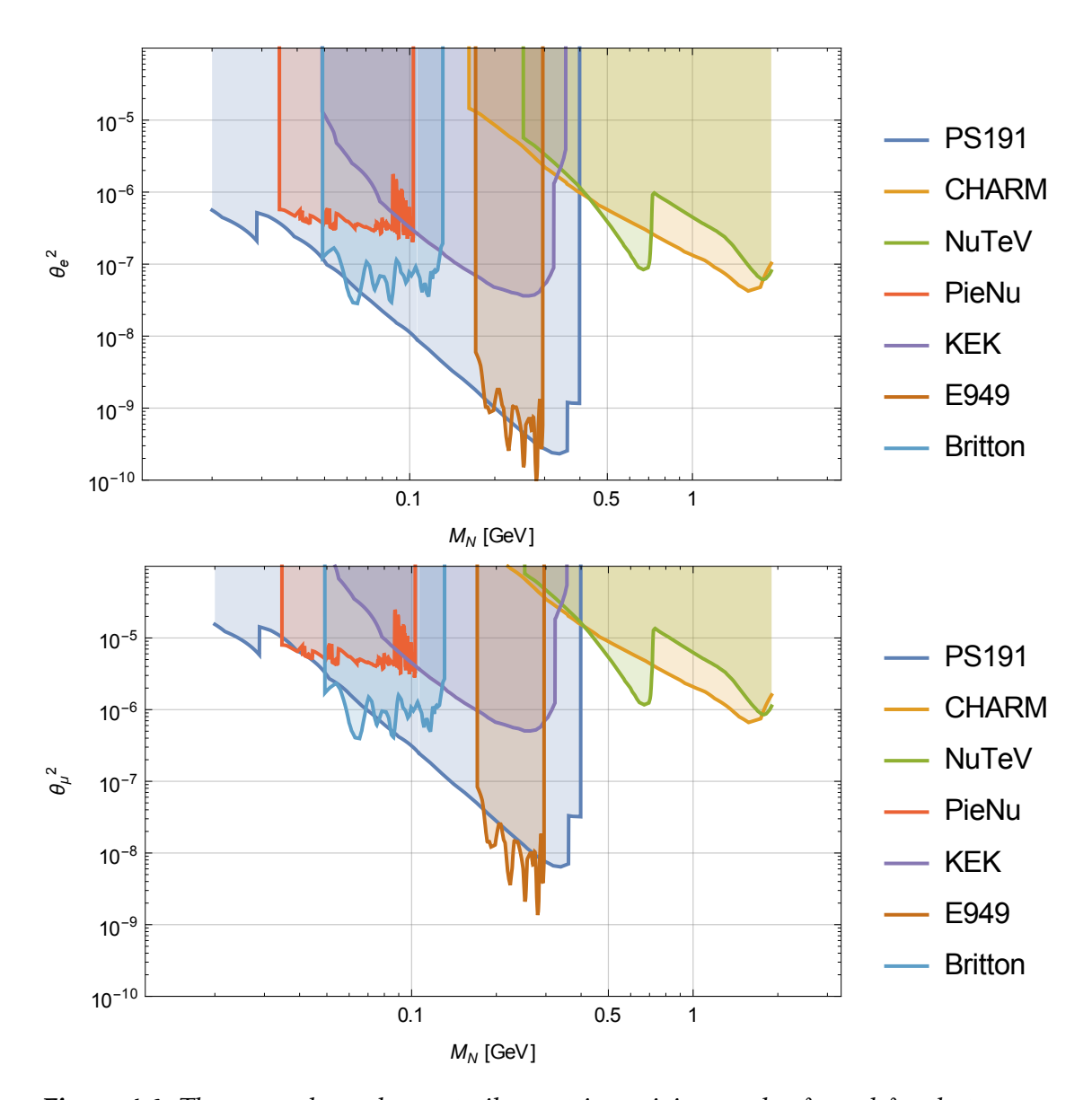


**Figure 4.6:** The upper bounds on sterile neutrino mixing angles  $\vartheta_e$  and  $\vartheta_\mu$ , that minimize the lifetime, as a function of its mass  $M_N$  for normal hierarchy. The data was taken from PS191 [21], CHARM [23], NuTeV [24], PieNu [15], KEK [18], E949 [17] and Britton et. al. [16].

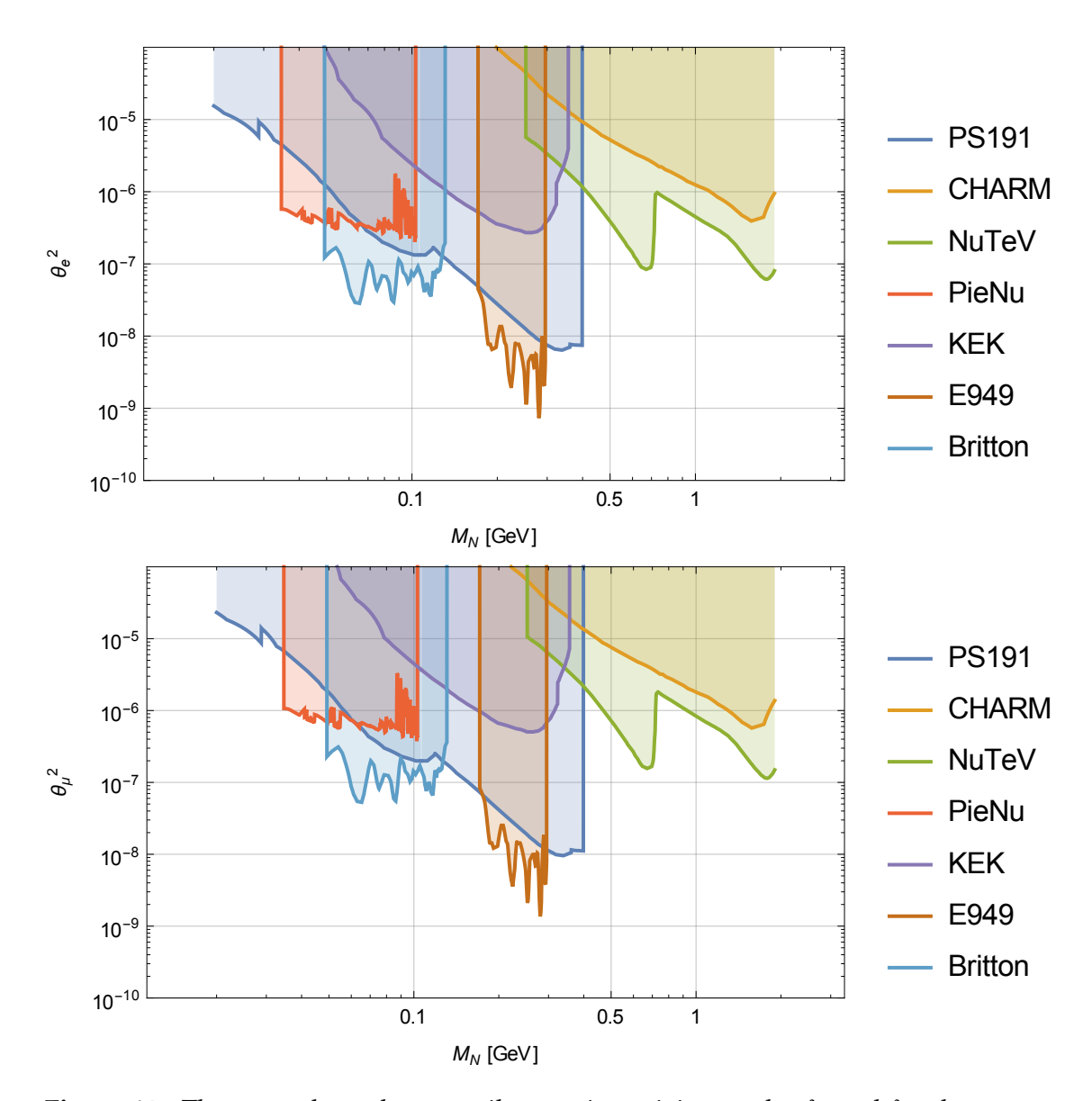
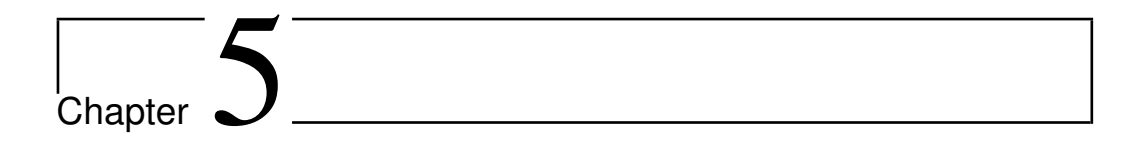


**Figure 4.7:** The upper bounds on sterile neutrino mixing angles  $\vartheta_e$  and  $\vartheta_\mu$ , that minimize the lifetime, as a function of its mass  $M_N$  for inverted hierarchy. The data was taken from PS191 [21], CHARM [23], NuTeV [24], PieNu [15], KEK [18], E949 [17] and Britton et. al. [16].



# Cosmological constraints

One of the main reasons for considering sterile neutrinos is to breach the gap between SM and cosmology. As already discussed, sterile neutrinos can provide a dark matter candidate and could be responsible for the generation of BAU through resonant leptogenesis. Models that try to explain these phenomena are therefore additionally constrained by cosmological observations. For example, the DM candidate should be relatively light  $\mathcal{O}(\text{keV})$  and extremely feebly interacting, so same particles could not explain neutrino masses and oscillations. On the other hand, for successful BAU mechanism with sterile neutrinos below the electroweak scale, two mass degenerate states are needed, for which upper and lower bound on coupling strength (or lifetime) can be obtained. Additionally, such extensions of the SM should not spoil the predictions of Big Bang nucleosynthesis (BBN), which combines particle physics and cosmology to describe the abundances of primordial nuclei. its predictions are in excellent agreement with the observations, however presence of sterile neutrinos could spoil them. For the considered model with two  $\mathcal{O}(\text{GeV})$  mass degenerate sterile neutrinos the relevant constraints on lifetime come from BBN and resonant leptogenesis, as will be presented in this chapter.

BBN and the influence of sterile neutrinos on it will be discussed in Section 5.1. This is be followed by a brief description of resonant leptogenesis, in Section 5.2. The cosmological constraints on sterile neutrinos are discussed only qualitatively, while corresponding bounds on lifetime taken from [5, 25, 26] are presented in Figure 6.1.

### 5.1 Big Bang nucleosynthesis

One of the major successes of modern cosmology and particle physics is the ability to describe the formation of primordial atomic nuclei in the early Universe. This process is known as the Big Bang nucleosynthesis and depends only on the initial conditions, while the rest is set by the known physics. Cosmology is important because it describes the evolution of the Universe's content while the BBN was taking place, while the particle abundances and interactions are essentially set by the SM. The only free parameter  $\eta_B = \frac{n_B}{n_\gamma}$ , the baryons per photon ratio which effectively measures they baryon asymmetry, can be determined from the CMB observations and sky surveys. The predicted nuclei abundances are in excellent agreement with independent observations of dwarf galaxies, where the effects of stellar nucleosynthesis are negligible, or extremely old objects like quasars.

The early Universe consisted of primordial plasma, which before BBN contained free protons and neutrons in thermal equilibrium. Due to relatively low particle density (compared to the one in stars) the only heavier element that could have formed was deuterium D, which has characteristically low binding energy. Therefore significant amounts of D could only be produced when the temperature of the Universe dropped below  $T_{BBN} \approx 70$  keV. At that point the hight energy photons, which could disassociate the D, became rare enough, allowing for heavier nuclei to be formed through fusion. At approximately the same time neutrons decoupled from primordial plasma and started decaying, putting an upper limit on the amount of D that could have been produced. The resulting abundances of all nuclei therefore strongly depend on the exact timing of neutron freeze-out and  $\eta_B$ , which is related to the temperature when D production became effective.

The existence of sterile neutrinos could effect the process of BBN in multiple ways. First of all, active neutrinos distribution could deviate from the thermal spectrum due to their production is sterile neutrino decays. This would effect proton and neutron abundances, which are in equilibrium defined by the following processes

$$n + e^{+} \leftrightarrow \bar{\nu}_{e} + p^{+}$$

$$n + \nu_{e} \leftrightarrow p^{+} + e^{-}$$
(5.1)

As a result, the produced amount of *D* (and subsequently all other nuclei) would change, making BBN inconsistent with the observations. Similarly, if sterile neutrinos would have decayed when the low energy active neutri-

nos was already decoupled, they would have heated the equilibrium part of plasma and again spoil BBN predictions. Additionally, sterile neutrinos could influence the thermal history of the Universe by changing its energy density, which would have an effect on the timing of neutron freeze-out and D production. All of these problems are avoided if sterile neutrino lifetimes are  $\tau \leq 0.1s$  [25]. In this way they would decay early enough for their effects to be washed out by thermal equilibrium before BBN took place.

### 5.2 Resonant leptogenesis

The origin of BAU poses an open question to modern cosmology and particle physics. In 1967 A. Sakharov [27] established three conditions, which need to be fulfilled in order for the Universe to generate baryon asymmetry. They are

- 1. Baryon number *B* must be violated
- 2. C and CP symmetry must be violated
- 3. The asymmetry must be produced out of thermal equilibrium

All of these conditions are fulfilled within the SM, however there is no know mechanism that could produce the observed amount of BAU. To be more precise, the experimentally measured Higgs mass excludes firstorder phase transition which is needed for departure from thermal equilibrium. Additionally, the CP violating effects in the SM are too small to generate enough asymmetry to explain the observations. The nonconservation ob B in the SM is only possible through anomalous electroweak field configurations, known as sphalerons. They allow the sum of lepton and baryon number, (L + B), to be violated, while (L - B) remains conserved. Sphalerons can occur at temperatures above  $T_{sph} \approx 100$ GeV, therefore baryon asymmetry could have been generated through lepton asymmetry at  $T \geq T_{sph}$ . This lead to different proposed mechanisms of baryogenesis through leptogenesis, among which is also the resonant leptogenesis. It is applicable for the considered case of two sterile neutrinos with nearly degenerate masses in  $\mathcal{O}(\text{GeV})$  [3, 4]. Sterile neutrinos are assumed to be first produced at reheating, after the cosmic inflation, like all SM particles. However, their production rate must be small due to their weak coupling and therefore they would need some time to enter thermal equilibrium with the surrounding plasma. If sterile neutrinos were out of thermal equilibrium all the way down to  $T_{sph}$ , then the coherent oscillations between the two states could produce lepton asymmetry. This lepton asymmetry could be then partly converted in baryon asymmetry through sphalerons. If sterile neutrinos would equilibrate before  $T_{syh}$  all the generated asymmetry would be washed out by thermal equilibrium, which restricts sterile neutrinos to  $\mathcal{O}$  GeV range. Additionally, sterile neutrinos could introduce an extra source of CP violation in the SM model. In their raw form this effects are again too small to explain the observed value of  $\eta_B$ , however they can be enhanced if the neutrinos are mass degenerate. More precisely, the frequency of oscillations between the heavy neutrino states  $\omega$  is proportional to their mass difference  $\Delta M$ . If the parameters are tuned, so that  $\omega \approx H(T_B)$ , where  $H(T_B)$  is the Hubble expansion rate during baryogenesis, maximum baryon asymmetry can be produced, which may be orders of magnitude larger then the observed value. Therefore sterile neutrino masses and their coupling strengths can be constrained, if one assumes the BAU was generated through resonant leptogenesis. Such mechanism puts a lower bound on sterile neutrino lifetimes, while upper bound can be obtained through the see-saw mechanism and BAU constraints on z parameter, which appears in Equations (2.12) and (2.13). More thorough discussion and updated constraints of this type can be found in [5].



# Conclusions

Sterile neutrino parameter space can be constrained by different experiments and observations, as discussed in previous chapters. Neutrino oscillations bound the ratios of the sterile-active mixing angles  $T_{\alpha}$ , defined in Equation (2.14). Such constraints were obtained, using recently published neutrino oscillation parameters [8]. The results are presented in Table 3.2, from where it can be seen that the constraints are slightly stronger then the ones based on older data. The change is the biggest for  $T_e$ , which is mainly due to stronger experimental evidence for  $\theta_{13} \neq 0$ . The correlations between the parameters were shown to have a negligible effect, compared to the uncertainties arising from unconstrained Majorana phases. Direct detection experiments provide an upper bound on the sterile-active neutrino mixing angles. The original interpretation of PS191 [21] and CHARM [23] experiment did not include neutral-current interactions, which were accounted for in my analysis. Additionally, the expected number of produced sterile neutrinos in CHARM experiment was calculated with higher precision, including also semi-leptonic decays of D mesons, which were neglected in original analysis. The resulting lower bound on sterile neutrino lifetimes, based on original and reinterpreted measurements of mixing angles, are presented in Figure 4.5. From there we can see that the minimum lifetime for IH gets increased by roughly an order of magnitude, while NH does not get effected by the re-analysis. Resonant leptogenesis, combined with the see-saw mechanism, can be used to infer a lower and upper bound on sterile neutrino lifetime. Furthermore, an independent upper bound on their lifetimes,  $\tau \leq 0.1$ s, can be imposed by BBN, since they should decay fast enough not to spoil its successful predictions.

All of the constraints, discussed above were combined into an exclusion plot presented in Figure 6.1. It was already shown [25, 26] that sterile

48 Conclusions

neutrinos with masses below pion mass ( $M_\pi \approx 140$  MeV) are disfavored. Recent peak search results [17] further excluded most of the parameter space below 300 MeV for NH, while for IH all  $M_N \leq 300$  MeV are disfavored. For higher masses the strongest constraints come from resonant leptogenesis and see-saw mechanism, since the experimental bounds in that range are much weaker. This will hopefully change in the near future with next generation of accelerator experiments. The most promising is the proposed Search for Hidden Particles (SHiP) [29] at the CERN SPS beam. It is expected to probe most of the unrestricted parameter space up to  $M_N \approx 2$  GeV. This range is phenomenologically the most interesting, since it coincides with all other lepton masses, however sterile neutrino masses could be much larger.

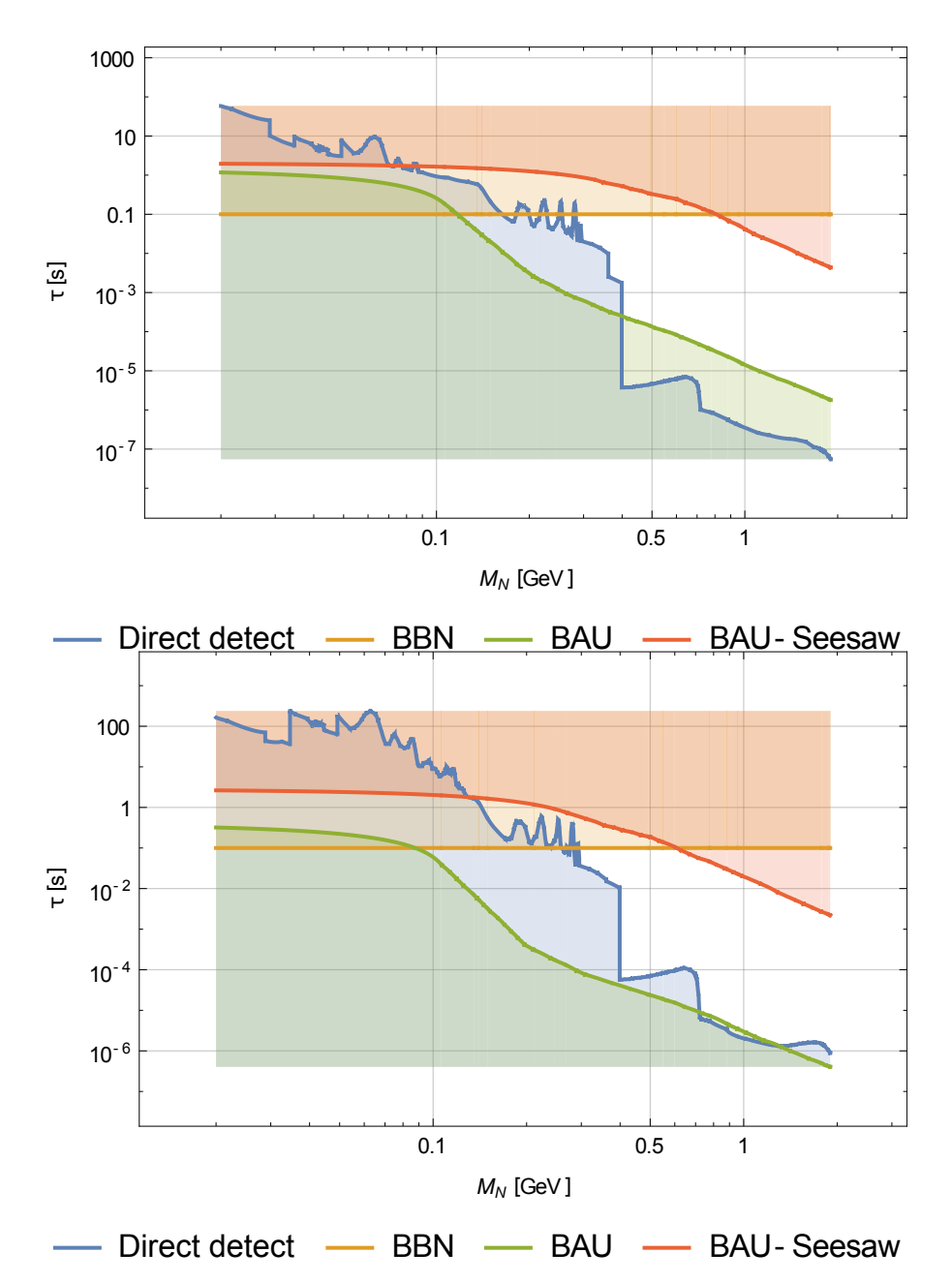


**Figure 6.1:** The combined bounds on sterile neutrino lifetimes  $\tau$  as a function of their mass  $M_N$ . The blue line represents the lower bounds coming from direct detection experiments and yellow line the upper bounds from BBN. The lower bound, derived purely from resonant leptogenesis is marked green, while the upper bound inferred from BAU and see-saw constraints is marked red. The top plot is for normal and bottom one for inverted hierarchy.



# Chi-squared test

The  $\chi^2$  test is a statistical hypothesis tests, which us tells how well does a certain hypothesis (i.e. theoretical prediction) fit the observational data. In case of neutrino oscillations the theoretical predictions vary as we change the oscillation parameters allowing us to find a set, which fits the best to the measurements. Furthermore, through the  $\chi^2$  distribution we can evaluate the confidence level (CL) of a certain set of parameters.

Having a set of N observables with corresponding experimental values  $\{R_n^{exp}\}$ , theoretical predictions  $\{R_n^{the}\}$  and uncorrelated errors  $\{u_n\}$  and K correlated errors  $\{c_n^k\}$  from independent sources, where  $n \in [1, N]$  and  $k \in [1, K]$ , we can evaluate the  $\chi^2$  function in the following way

$$\chi^{2} = \sum_{n,m=1}^{N} (R_{n}^{exp} - R_{n}^{the}) (\sigma_{nm}^{2})^{-1} (R_{m}^{exp} - R_{m}^{the})$$

$$\sigma_{nm}^{2} = \delta_{nm} u_{n} u_{m} + \sum_{k=1}^{K} c_{n}^{k} c_{m}^{k}$$
(A.1)

This is the so called covariance approach of calculating the  $\chi^2$ . There exists also the pull approach, however it can be shown the two are strictly equal [30]. The pull approach turns out to be more useful in practice, since it is less computational demanding and it allows splitting  $\chi^2$  into the contributions from residuals of the observable and of the systematics. In order to calculate it, we first introduce set of new Gaussian variables  $\{\xi_k\}$  and preform a shift of the difference between measurements and theoretical

52 Chi-squared test

predictions by  $\xi_k c_n^k$  and then minimize the  $\chi_{pull}$  with respect to  $\{\xi_k\}$ 

$$R_{n}^{exp} - R_{n}^{the} \rightarrow R_{n}^{exp} - R_{n}^{the} - \sum_{k=1}^{K} \xi_{k} c_{n}^{k}$$

$$\chi_{pull}^{2} = \min_{\{\xi_{k}\}} \left[ \sum_{n=1}^{N} \frac{(R_{n}^{exp} - R_{n}^{the} - \sum_{k=1}^{K} \xi_{k} c_{n}^{k})^{2}}{u_{n}} + \sum_{k=1}^{K} \xi_{k}^{2} \right]$$
(A.2)

This gives us a set of "pulls" of systematics  $\{\bar{\xi}_k\}$ , for which  $\chi^2$  is minimal. We can now rewrite the  $\chi^2$ , by splitting it into a contribution from observation and systematics residuals

$$\bar{x}_n = \frac{R_n^{exp} - (R_n^{the} + \sum_{k=1}^K \bar{\xi}_k c_n^k)}{u_n}$$

$$\chi^2 = \sum_{n=1}^N \bar{x}_n^2 + \sum_{k=1}^K \bar{\xi}_k^2 = \chi_{obs}^2 + \chi_{sys}^2$$
(A.3)

In case of neutrino oscillations experiments the rate of neutrino detection is usually measured. The expression for theoretical prediction of the event rate depends on the type of experiment and detection methods, but in general takes the following form

$$R_n^{the}(\mathbf{p}) = \int_{E_{min}}^{E_{max}} dE \; \Phi_{\nu}(E) \sigma(E) P_{\nu_{\alpha} \to \nu_{\beta}}(E|\mathbf{p})$$

$$\mathbf{p} = (\theta_{12}, \theta_{13}, \theta_{23}, \delta_{CP}, \Delta m_{21}^2, \Delta m_{31}^2) \tag{A.4}$$

where  $\Phi_{\nu}(E)$  is the neutrino flux,  $\sigma(E)$  the process cross-section (here the efficiency of detector is included in  $\sigma$ ) and  $P_{\nu_{\alpha} \to \nu_{\beta}}(E|\mathbf{p})$  is the oscillation probability between the relevant neutrino flavors. All of these quantities generally depend on energy E, while the oscillation probability also depends on the values of the oscillation parameters, collected in  $\mathbf{p}$ .

Using the above allows us to evaluate the  $\chi^2$  function. The global best fit is given by minimization with respect to all parameters **p** 

$$\chi_{global}^2 = \min_{\mathbf{p}} \chi^2(\mathbf{p}) \tag{A.5}$$

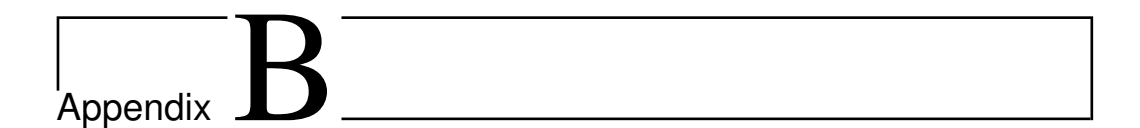
The real advantage of using the  $\chi^2$  test becomes clear when we ask ourselves, what are the certainty intervals for the oscillation parameters. They can be determined by looking at the deviation of  $\chi^2$  for some particular parameters from the global best fit value

$$\Delta \chi^2(\mathbf{p}) = \chi^2(\mathbf{p}) - \chi^2_{global} \tag{A.6}$$

 $\Delta\chi^2$  can be then related to confidence levels through the  $\chi^2_k$  distribution with the corresponding number of degrees of freedom k. We are often interested in the certainty interval of only a few of the six oscillation parameters. These can be obtained by marginalizing  $\chi^2$  with respect to the parameters we are not interested in

$$\chi^{2}(\{p_{i}\}) = \min_{\{p_{j}\} \notin \{p_{i}\}} \chi^{2}(\mathbf{p})$$

$$\Delta \chi^{2}(\{p_{i}\}) = \chi^{2}(\{p_{i}\}) - \chi^{2}_{global}$$
(A.7)



# Scattering processes involving sterile neutrino

Sterile neutrinos N are coupled to other SM only through mixing with active neutrinos  $\nu_{\alpha}$ . Therefore, all scattering processes involving sterile neutrinos will consist of mixing between N and  $\nu_{\alpha}$  or  $\bar{\nu}_{\alpha}$ , for which the probability is proportional to  $\theta_{\alpha}^2$ . Other parts of the scattering processes can be computed using the ordinary perturbation theory for weak interactions. Since sterile neutrinos are expected to be heavy and they have no conserved quantum charge they must be unstable particles. Fermi theory is used to determine the decay width of two and three body decays of sterile neutrinos, which are important for correct interpretation of experimental searches. Additionally, branching ratios for sterile neutrino production in pure leptonic and semi-leptonic decays of mesons are evaluated. The semi-leptonic decays were usually neglected in the analysis of experiments, therefore it allows for stronger bounds to be imposed on sterile-active neutrino mixing angles.

### **B.1** Sterile neutrino decays

### **B.1.1** Three body decay modes

The most important three body decays of sterile neutrinos are the decays into three leptons of the SM. The possible scatterings are

$$N \to \nu_{\alpha} \bar{\nu}_{\beta} \nu_{\beta}$$
 (B.1)

$$N \to l_{\alpha}^{-} l_{\beta}^{+} \nu_{\beta} \tag{B.2}$$

$$N \to \nu_{\alpha} l_{\beta}^- l_{\beta}^+ \tag{B.3}$$

The calculations of decay widths for these processes are similar, however decay (B.1) is somewhat easier to compute, since one can neglect the active neutrino masses. In what follows I will reproduce some of the results for decay width given in [31], beginning with process depicted in Figure B.1. To do this one needs to consider two distinct cases, one where  $\alpha = \beta$  and the other, where  $\alpha \neq \beta$ .

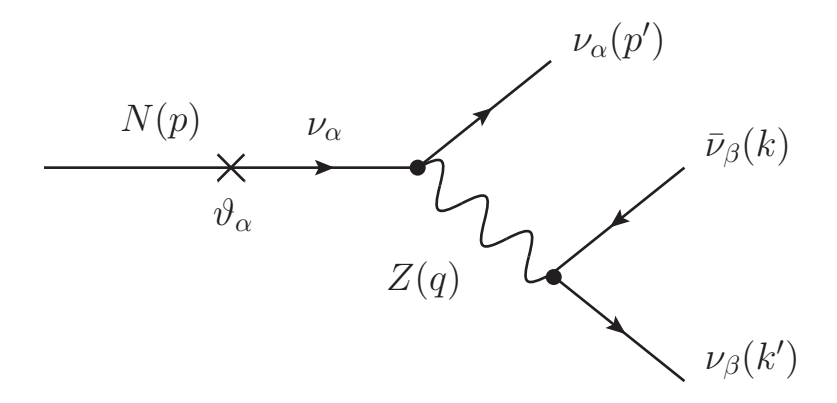


**Figure B.1:** The Feynman diagram of the three body  $N \to \nu_{\alpha} \bar{\nu}_{\beta} \nu_{\beta}$  decay

Lets first consider the  $\alpha \neq \beta$  process. The amplitude for the process is

$$iM_{\alpha \neq \beta} = \vartheta_{\alpha} \bar{u}^{s}(p') \left( -\frac{ig}{2\cos\vartheta_{W}} \gamma^{\mu} P_{L} \right) u^{s'}(p)$$

$$\cdot \left( -\frac{ig_{\mu\nu}}{q^{2} - M_{Z}^{2}} \right) \bar{u}^{r}(k) \left( -\frac{ig}{2\cos\vartheta_{W}} \gamma^{\mu} P_{L} \right) v^{r'}(k')$$

$$= \sqrt{2}iG_{F} \vartheta_{\alpha} \left( \bar{u}^{s}(p') \gamma^{\mu} P_{L} u^{s'}(p) \right) \left( \bar{u}^{r}(k) \gamma_{\mu} P_{L} v^{r'}(k') \right)$$
(B.4)

In the second line we assumed that sterile neutrino is much lighter then the  $Z^0$  boson, i.e  $q \ll M_Z$ , and used  $\sqrt{2}G_F = (\frac{g}{2M_Z\cos\theta_W})^2$ . The averaged scattering probability is then

$$\left\langle |M_{\alpha\neq\beta}|^{2} \right\rangle = \frac{1}{2} \sum_{s} \sum_{s',r,r'} |M_{\alpha\neq\beta}|^{2}$$

$$= G_{F}^{2} \vartheta_{\alpha}^{2} \sum_{s',r,r'} \sum_{s} \left( \bar{u}^{s}(p') \gamma^{\mu} P_{L} u^{s'}(p) \bar{u}^{s'}(p) \gamma^{\nu} P_{L} u^{s}(p') \right)$$

$$\cdot \left( \bar{u}^{r}(k) \gamma_{\mu} P_{L} v^{r'}(k') \bar{v}^{r'}(k') \gamma_{\nu} P_{L} u^{r}(k) \right)$$

$$= G_{F}^{2} \vartheta_{\alpha}^{2} \operatorname{Tr} \left[ p' \gamma^{\mu} p \gamma^{\nu} P_{L} \right] \operatorname{Tr} \left[ k \gamma_{\mu} k' \gamma_{\nu} P_{L} \right]$$

$$= 4G_{F}^{2} \vartheta_{\alpha}^{2} \left( p'^{\mu} p^{\nu} + p'^{\nu} p^{\mu} - g^{\mu\nu}(p' \cdot p) + i \epsilon^{\alpha\mu\beta\nu} p'_{\alpha} p_{\beta} \right)$$

$$\cdot \left( k_{\mu} k'_{\nu} + k_{\nu} k'_{\mu} - g_{\mu\nu}(k \cdot k') + i \epsilon_{\sigma\mu\rho\nu} k_{\sigma} k'_{\rho} \right)$$

$$= 16G_{F}^{2} \vartheta_{\alpha}^{2}(p' \cdot k)(p \cdot k') \tag{B.5}$$

To obtain the decay rate, we can use the standard three body decay ansatz [32]

$$d\Gamma = \frac{1}{16M^{2}(2\pi)^{5}} \left\langle |M|^{2} \right\rangle |p_{1}^{*}||p_{3}|dm_{12}d\Omega_{1}^{*}d\Omega_{3}$$

$$|p_{1}^{*}| = \frac{\left[ (m_{12}^{2} - (m_{1} + m_{2})^{2})(m_{12}^{2} - (m_{1} - m_{2})^{2}) \right]^{1/2}}{2m_{12}} = \frac{m_{12}}{2}$$

$$|p_{3}| = \frac{\left[ (M^{2} - (m_{12} + m_{3})^{2})(M^{2} - (m_{12} - m_{3})^{2}) \right]^{1/2}}{2M} =$$

$$= \frac{m_{N}}{2} (1 - \frac{m_{12}^{2}}{m_{N}^{2}})$$
(B.6)

In (B.6) M stands for the mass of initial particle, which is in our case the sterile neutrino mass  $m_N$ , while the masses of the active neutrinos  $(m_1, m_2, m_3)$  are negligible.  $m_{12}$  is defined as  $m_{ij}^2 = p_{ij}^2 = (p_i + p_j)^2$ , where i and j are the indexes of the particles produced by the decay. By choosing  $p_1 = p'$ ,  $p_2 = k$  and  $p_3 = k'$  and moving to the CMS of the decaying particle we can rewrite the result of (B.5) using the following relations

$$m_{12}^2 = (p_1 + p_2)^2 = (p' + k)^2 = p'^2 + k^2 + 2p' \cdot k = 2p' \cdot k$$
  

$$\Rightarrow p' \cdot k = \frac{m_{12}^2}{2}$$
(B.7)

$$p \cdot k' = m_N |k'| = m_N |p_3| = \frac{m_N^2}{2} (1 - \frac{m_{12}^2}{m_N^2})$$
 (B.8)

This yields

$$\left\langle |M_{\alpha \neq \beta}|^2 \right\rangle = 4G_F^2 \vartheta_{\alpha}^2 m_N^2 m_{12}^2 (1 - \frac{m_{12}^2}{m_N^2})$$
 (B.9)

Since the expression B.9 depends solely on  $m_{12}$  the space angle integrals become trivial, i.e.  $\int d\Omega_1^* = \int d\Omega_3 = 4\pi$ . Using the above, the expression for decay width yields

$$d\Gamma_{\alpha \neq \beta} = \frac{G_F^2 m_N}{16(2\pi)^5} \vartheta_{\alpha}^2 m_{12}^3 (1 - \frac{m_{12}^2}{m_N^2})^2 dm_{12} d\Omega_1^* d\Omega_3$$

$$\Gamma_{\alpha \neq \beta} = \frac{G_F^2 m_N}{4(2\pi)^3} \vartheta_{\alpha}^2 \int_0^{m_N} m_{12}^3 (1 - \frac{m_{12}^2}{m_N^2})^2 dm_{12}$$

$$= \frac{G_F^2 m_N^5}{768\pi^3} \vartheta_{\alpha}^2$$
(B.10)

In the case where  $\alpha = \beta$  we get interference of two indistingishable processes, namely the one shown in Figure B.1 and analogous one, where  $\nu_{\alpha}(p')$  and  $\nu_{\beta}(k')$  are interchanged. The scattering amplitude is then the sum of the two processes (here it is important to note that the amplitudes come with a different sign), written out explicitly

$$iM_{\alpha=\beta} = iM_{1} + iM_{2}$$

$$= \sqrt{2}iG_{F}\vartheta_{\alpha} \left[ \left( \bar{u}^{s}(p')\gamma^{\mu}P_{L}u^{s'}(p) \right) \left( \bar{u}^{r}(k)\gamma_{\mu}P_{L}v^{r'}(k') \right) - \left( \bar{u}^{r}(k)\gamma^{\mu}P_{L}u^{s'}(p) \right) \left( \bar{u}^{s}(p')\gamma_{\mu}P_{L}v^{r'}(k') \right) \right]$$
(B.11)

The averaged scattering probability is then

$$\langle |M_{\alpha=\beta}|^2 \rangle = \frac{1}{2} \sum_{s} \sum_{s',r,r'} |M_{\alpha=\beta}|^2$$

$$= \frac{1}{2} \sum_{s} \sum_{s',r,r'} \left( |M_1|^2 - M_1 M_2^{\dagger} - M_1^{\dagger} M_2 + |M_2|^2 \right)$$
(B.12)

At this point we can simplify the calculation, by realizing that the  $|M_1|^2$  and  $|M_2|^2$  terms yield the same result as the  $|M_{\alpha\neq\beta}|^2$  (with corresponding substitutions of momenta), so we only need to consider the cross terms,

 $M_1M_2^{\dagger}$  and  $M_1^{\dagger}M_2$ . The averaged scattering probability for them is

$$\langle |M_{cross}|^{2} \rangle = \frac{1}{2} \sum_{s} \sum_{s',r,r'} \left( M_{1} M_{2}^{\dagger} + M_{1}^{\dagger} M_{2} \right)$$

$$= -G_{F}^{2} \vartheta_{\alpha}^{2} \sum_{s} \sum_{s',r,r'} \left[ \left( \bar{u}^{s}(p') \gamma^{\mu} P_{L} u^{s'}(p) \bar{u}^{s'}(p) \gamma^{\nu} P_{L} u^{r}(k) \right) \right.$$

$$\cdot \bar{u}^{r}(k) \gamma_{\mu} P_{L} v^{r'}(k') \bar{v}^{r'}(k') \gamma_{\nu} P_{L} u^{s}(p') \right)$$

$$- \left( \bar{u}^{r}(k) \gamma^{\mu} P_{L} u^{s'}(p) \bar{u}^{s'}(p) \gamma^{\nu} P_{L} u^{s}(p') \right.$$

$$\cdot \bar{u}^{s}(p') \gamma_{\mu} P_{L} v^{r'}(k') \bar{v}^{r'}(k') \gamma_{\nu} P_{L} u^{r}(k) \right) \right]$$

$$= 2G_{F}^{2} \vartheta_{\alpha}^{2} \left( \operatorname{Tr} \left[ p' k \gamma^{\nu} p k' \gamma_{\nu} P_{L} \right] + \operatorname{Tr} \left[ k p' \gamma^{\nu} p k' \gamma_{\nu} P_{L} \right] \right)$$

$$= 8G_{F}^{2} \vartheta_{\alpha}^{2}(p \cdot k') \left( \operatorname{Tr} \left[ p' k P_{L} \right] + \operatorname{Tr} \left[ k p' P_{L} \right] \right)$$

$$= 32G_{F}^{2} \vartheta_{\alpha}^{2}(p \cdot k') (p' \cdot k)$$

$$(B.13)$$

In this calculation I used the following properties of the  $\gamma$ -matrices [33]

$$\begin{split} \gamma^{\alpha}\gamma^{\mu}\gamma^{\nu}\gamma^{\rho}\gamma_{\alpha} &= -2\gamma^{\rho}\gamma^{\nu}\gamma^{\mu} \\ \gamma^{\alpha}\gamma^{\mu}\gamma^{\nu}\gamma_{\alpha} &= 4g^{\mu\nu} \\ \operatorname{Tr}\left[\gamma^{\mu}\gamma^{\nu}\right] &= 4g^{\mu\nu} \\ \operatorname{Tr}\left[\gamma^{\mu}\gamma^{\nu}\gamma^{5}\right] &= 0 \end{split} \tag{B.14}$$

The result (B.13) is almost identical to the one we got for the  $\alpha \neq \beta$  case; the averaged squared matrix element is bigger by a factor 2, however there is an additional factor of  $\frac{1}{2!}$  in (B.6) (the symmetry factor of the process), therefore the decay widths must be the same. The total decay width for  $\alpha = \beta$  therefore equals to

$$\Gamma_{\alpha=\beta} = \Gamma(|M_1|^2) + \Gamma(|M_2|^2) + \Gamma(|M_{cross}|^2)$$

$$= 3\Gamma_{\alpha\neq\beta} = \frac{G_F^2 m_N^5}{256\pi^3} \vartheta_{\alpha}^2$$
(B.15)

The total decay width for sterile neutrino decaying in three active neutrinos is then

$$\Gamma(N \to \nu_{\alpha} \bar{\nu}_{\beta} \nu_{\beta}) = \Gamma_{\alpha \neq \beta} + \Gamma_{\alpha = \beta} = \frac{G_F^2 m_N^5}{192 \pi^3} \vartheta_{\alpha}^2$$
 (B.16)

The decay widths for other three body decays are [31]

$$\Gamma(N \to l_{\alpha \neq \beta}^{-} l_{\beta}^{+} \nu_{\beta}) = \frac{G_F^2 m_N^5}{192 \pi^3} \vartheta_{\alpha}^2 (1 - 8x^2 + 8x^6 - x^8 - 12x^4 \log x^2)$$

$$x = \frac{\max[m_{l_{\alpha}}, m_{l_{\beta}}]}{m_N}$$
(B.17)

$$\Gamma(N \to \nu_{\alpha} l_{\beta}^{+} l_{\beta}^{-}) = \frac{G_{F}^{2} m_{N}^{5}}{192 \pi^{3}} \vartheta_{\alpha}^{2} \left[ (C_{1}(1 - \delta_{\alpha\beta}) + C_{3}\delta_{\alpha\beta}) \right]$$

$$\cdot \left( (1 - 14x^{2} - 2x^{4} - 12x^{6}) \sqrt{1 - 4x^{2}} + 12x^{4}(x^{4} - 1)L \right)$$

$$+4(C_{2}(1 - \delta_{\alpha\beta}) + C_{4}\delta_{\alpha\beta})$$

$$\cdot \left( x^{2}(2 + 10x^{2} - 12x^{4}) + \sqrt{1 - 4x^{2}} + 6x^{4}(1 - 2x^{2} + 2x^{4})L \right) \right]$$

$$L = \log \left[ \frac{1 - 3x^{2} - (1 - x^{2})\sqrt{1 - 4x^{2}}}{x^{2}\left(1 + \sqrt{1 - 4x^{2}}\right)} \right] , \quad x = \frac{m_{l}}{m_{N}}$$

$$(B.18)$$

### B.1.2 Two body decay modes

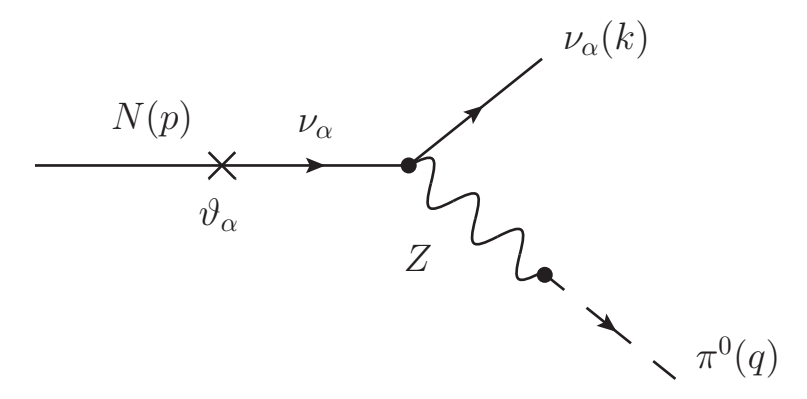


**Figure B.2:** The Feynman diagram of the two body  $N \to \pi^0 \nu_{\alpha}$  decay

First let us consider decay of sterile neutrinos into neutral meson  $\pi^0$  and an active neutrino  $\nu_{\alpha}$ , depicted in Figure B.2. The scattering amplitude for

the process is

$$iM = \vartheta_{\alpha}\bar{u}^{s}(k) \left( -\frac{ig}{2\cos\vartheta_{W}} \gamma^{\mu} P_{L} \right) u^{s'}(p) \left( -\frac{ig_{\mu\nu}}{q^{2} - M_{Z}^{2}} \right)$$

$$\left( -\frac{ig}{2\sqrt{2}\cos\vartheta_{W}} \gamma^{\mu} P_{L} \right) f_{\pi} q_{\mu}$$

$$= -iG_{F} f_{\pi} \vartheta_{\alpha} \left( \bar{u}^{s}(k) \gamma^{\mu} P_{L} u^{s'}(p) \right) q_{\mu}$$
(B.19)

from where we can calculate its average amplitude squared

$$\langle |M|^{2} \rangle = \frac{1}{2} \sum_{s,s'} |M|^{2}$$

$$= \frac{G_{F}^{2} f_{\pi}^{2}}{2} \vartheta_{\alpha}^{2} \sum_{s,s'} \left( \bar{u}^{s}(k) \gamma^{\mu} P_{L} u^{s'}(p) \bar{u}^{s'}(p) \gamma^{\nu} P_{L} u^{s}(k) \right) q_{\mu} q_{\nu}$$

$$= \frac{G_{F}^{2} f_{\pi}^{2}}{2} \vartheta_{\alpha}^{2} \operatorname{Tr} \left[ k \gamma^{\mu} (p + m_{N}) \gamma^{\nu} P_{L} \right] q_{\mu} q_{\nu}$$

$$= G_{F}^{2} f_{\pi}^{2} \vartheta_{\alpha}^{2} \left( 2(p \cdot q)(k \cdot q) - (k \cdot p) q^{2} \right)$$
(B.20)

We can simplify this expression by using that  $p^2 = m_N^2$ ,  $q^2 = m_\pi^2$ ,  $k^2 = 0$  and the following kinematic equations

$$p \cdot q = p \cdot (p - k) = m_N^2 - p \cdot q$$

$$k \cdot q = k \cdot (p - k) = p \cdot k$$

$$k \cdot q = (p - q) \cdot q = p \cdot q - m_\pi^2$$

$$\Rightarrow p \cdot k = q \cdot k = \frac{1}{2}(m_N^2 - m_\pi^2)$$

$$\Rightarrow p \cdot q = \frac{1}{2}(m_N^2 + m_\pi^2)$$
(B.21)

The averaged scattering probability then takes the following form

$$\left\langle |M|^2 \right\rangle = \frac{G_F^2 f_\pi^2}{2} \vartheta_\alpha^2 m_N^4 (1 - \frac{m_\pi^2}{m_N^2})$$
 (B.22)

To obtain the decay rate, I used the standard two-body decay ansatz [32].

$$d\Gamma = \frac{1}{32\pi^2} \langle |M|^2 \rangle \frac{|p_1|}{M^2} d\Omega$$

$$E_1 = \frac{M^2 - m_2^2 + m_1^2}{2M}$$
(B.23)

In our case the initial particle is the sterile neutrino, therefore  $M=m_N$ , and we can choose the decay particle 1 to be the neutrino  $\nu_{\alpha}$ , so  $|p_1| \approx E_1 = \frac{m_N}{2}(1-\frac{m_{\pi}^2}{m_N^2})$ . Since  $\langle |M|^2 \rangle$  is a constant, the space angle integral is simply  $\int d\Omega = 4\pi$ . Plugging this in (B.23) we obtain

$$\Gamma(N \to \pi^0 \nu_{\alpha}) = \frac{G_F^2 f_{\pi}^2}{32\pi} \vartheta_{\alpha}^2 m_N^3 (1 - \frac{m_{\pi}^2}{m_N^2})^2$$
 (B.24)

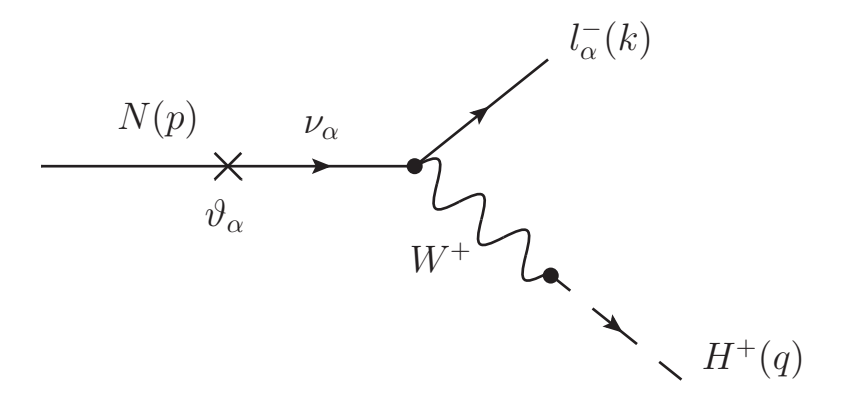


**Figure B.3:** The Feynman diagram of the two body  $N \to H^+ l_{\alpha}^-$  decay

Now let us consider decay of sterile neutrinos into a charged meson and a lepton, depicted in Figure B.3. The scattering amplitude for the process is

$$iM = \vartheta_{\alpha} \bar{u}^{s}(k) \left( -\frac{ig}{\sqrt{2}} \gamma^{\mu} P_{L} \right) u^{s'}(p) \left( -\frac{ig_{\mu\nu}}{q^{2} - M_{W}^{2}} \right) \left( \frac{g}{2\sqrt{2}} \right) V_{H} f_{\pi} q_{\mu}$$

$$= -\sqrt{2} G_{F} f_{H} V_{H} \vartheta_{\alpha} \left( \bar{u}^{s}(k) \gamma^{\mu} P_{L} u^{s'}(p) \right)$$
(B.25)

from where we can calculate its average amplitude squared

$$\langle |M|^{2} \rangle = \frac{1}{2} \sum_{s,s'} |M|^{2}$$

$$= G_{F}^{2} f_{H}^{2} |V_{H}|^{2} \vartheta_{\alpha}^{2} \sum_{s,s'} \left( \bar{u}^{s}(k) \gamma^{\mu} P_{L} u^{s'}(p) \bar{u}^{s'}(p) \gamma^{\nu} P_{L} u^{s}(k) \right) q_{\mu} q_{\nu}$$

$$= G_{F}^{2} f_{H}^{2} |V_{H}|^{2} \vartheta_{\alpha}^{2} \operatorname{Tr} \left[ (k + m_{l}) \gamma^{\mu} P_{L}(p + m_{N}) \gamma^{\nu} P_{L} \right] q_{\mu} q_{\nu}$$

$$= G_{F}^{2} f_{H}^{2} |V_{H}|^{2} \vartheta_{\alpha}^{2} \left( \operatorname{Tr} \left[ k \gamma^{\mu} p \gamma^{\nu} P_{L} \right] + m_{l} m_{N} \operatorname{Tr} \left[ \gamma^{\mu} \gamma^{\nu} P_{R} P_{L} \right] \right) q_{\mu} q_{\nu}$$

$$= G_{F}^{2} f_{H}^{2} |V_{H}|^{2} \vartheta_{\alpha}^{2} \left( k^{\mu} p^{\nu} + k^{\nu} p^{\mu} - g^{\mu\nu} p \cdot k + i \varepsilon^{\alpha \mu \beta \nu} k_{\alpha} p_{\beta} \right) q_{\mu} q_{\nu}$$

$$= 2G_{F}^{2} f_{H}^{2} |V_{H}|^{2} \vartheta_{\alpha}^{2} \left( 2(p \cdot q)(k \cdot q) - (k \cdot p) q^{2} \right)$$

$$(B.26)$$

Similarly as in the case of decay into  $\pi^0$ , we can simplify this expression by using that  $p^2 = m_N^2$ ,  $q^2 = m_H^2$ ,  $k^2 = m_l^2$  and the following kinematic equations

$$p \cdot q = p \cdot (p - k) = m_N^2 - p \cdot q$$

$$k \cdot q = k \cdot (p - k) = p \cdot k - m_l^2$$

$$k \cdot q = (p - q) \cdot q = p \cdot q - m_H^2$$

$$\Rightarrow p \cdot q = \frac{1}{2} (m_N^2 + m_H^2 - m_l^2)$$

$$\Rightarrow p \cdot k = \frac{1}{2} (m_N^2 + m_H^2 + m_l^2)$$

$$\Rightarrow q \cdot k = \frac{1}{2} (m_N^2 - m_H^2 - m_l^2)$$
(B.27)

The averaged scattering probability then takes the following form

$$\langle |M|^2 \rangle = G_F^2 f_H^2 |V_H|^2 \vartheta_\alpha^2 m_N^4 \cdot \left( \left( 1 - \frac{m_l^2}{m_N^2} \right)^2 - \frac{m_H^2}{m_N^2} \left( 1 + \frac{m_l^2}{m_N^2} \right) \right)$$
 (B.28)

Same as before, we use the standard two-body decay ansatz (B.23) to calculate the decay width. In this case both of the produced particles are massive, therefore

$$|p_1| = \frac{m_N}{2} \sqrt{(1 - \frac{(m_H - m_l)^2}{m_N^2})(1 - \frac{(m_H + m_l)^2}{m_N^2})}$$
(B.29)

Finally we obtain

$$\Gamma(N \to H^+ l_{\alpha}^-) = \frac{G_F^2 f_H^2 |V_H|^2}{16\pi} \vartheta_{\alpha}^2 m_N^3 \left( \left( 1 - \frac{m_l^2}{m_N^2} \right)^2 - \frac{m_H^2}{m_N^2} \left( 1 + \frac{m_l^2}{m_N^2} \right) \right)$$

$$\cdot \sqrt{\left( 1 - \frac{(m_H - m_l)^2}{m_N^2} \right) \left( 1 - \frac{(m_H + m_l)^2}{m_N^2} \right)}$$
(B.30)

with the relevant constants and CKM matrix elements  $V_H$  given in Table B.1.

**Table B.1:** Values of constants and relevant CKM matrix elements for the  $N \rightarrow H^+l^-_{\alpha}$  decays.

Analogously to the calculations above we can obtain the decay widths of other two body decays [7]

$$\Gamma(N \to \eta \nu_{\alpha}) = \frac{G_F^2 f_{\eta}^2}{32\pi} \vartheta_{\alpha}^2 m_N^3 \left( 1 - \frac{m_{\eta}^2}{m_N^2} \right)^2 
\Gamma(N \to \eta' \nu_{\alpha}) = \frac{G_F^2 f_{\eta'}^2}{32\pi} \vartheta_{\alpha}^2 m_N^3 \left( 1 - \frac{m_{\eta'}^2}{m_N^2} \right)^2 
\Gamma(N \to \rho^0 \nu_{\alpha}) = \frac{G_F^2 g_{\rho}^2}{16\pi} \vartheta_{\alpha}^2 \frac{m_N^3}{m_{\rho}^2} \left( 1 + 2 \frac{m_{\rho}^2}{m_N^2} \right) \left( 1 - \frac{m_{\rho}^2}{m_N^2} \right)^2 
\Gamma(N \to \rho^+ l_{\alpha}^-) = \frac{G_F^2 g_{\rho}^2 |V_{ud}|^2}{8\pi} \vartheta_{\alpha}^2 \frac{m_N^3}{m_{\rho}^2} \left( \left( 1 - \frac{m_l^2}{m_N^2} \right)^2 + \frac{m_{\rho}^2}{m_N^2} \left( 1 + \frac{m_l^2 - 2m_{\rho}^2}{m_N^2} \right) \right) 
\cdot \sqrt{\left( 1 - \frac{(m_{\rho} - m_l)^2}{m_N^2} \right) \left( 1 - \frac{(m_{\rho} + m_l)^2}{m_N^2} \right)}$$
(B.31)

where  $f_{\eta} = 1.2 f_{\pi}$ ,  $f_{\eta'} = -0.45 f_{\pi}$ ,  $g_{\rho} = 0.102 \ GeV^2$ .

## **B.2** Sterile neutrino production

#### **B.2.1** Pure leptonic meson decays

In all the considered experiments, sterile neutrinos were produced in meson decays. The dominant processes are two body leptonic and three body semi-leptonic decays of pseudo-scalar mesons. Let us first consider the two body decay leptonic decay of a charged pseudo-scalar meson  $H^+$  as presented in Figure B.4. It can be immediately seen that the process is symmetric to the two body decay of a sterile neutrino into charged meson and lepton, evaluated in Appendix B.1.2.

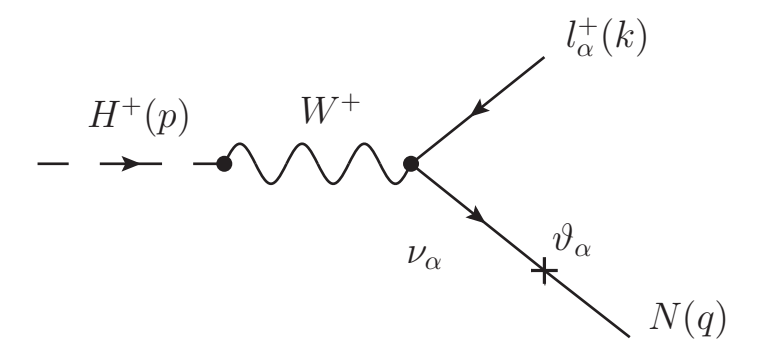


**Figure B.4:** The Feynman diagram of the two body  $H^+ \rightarrow l_{\alpha}^+ N$  decay

After analogous calculation the following decay width is obtained

$$\Gamma(H^{+} \to l_{\alpha}^{+} N) = \frac{G_{F}^{2} f_{H}^{2} |V_{H}|^{2}}{8\pi} \vartheta_{\alpha}^{2} m_{H}^{3} \left( \frac{m_{l}^{2}}{m_{H}^{2}} + \frac{m_{N}^{2}}{m_{H}^{2}} - \left( \frac{m_{l}^{2}}{m_{H}^{2}} - \frac{m_{N}^{2}}{m_{H}^{2}} \right)^{2} \right)$$

$$\cdot \sqrt{\left( 1 - \frac{(m_{l} - m_{N})^{2}}{m_{H}^{2}} \right) \left( 1 - \frac{(m_{l} + m_{N})^{2}}{m_{H}^{2}} \right)}$$
(B.32)

### **B.2.2** Semi-leptonic meson decays

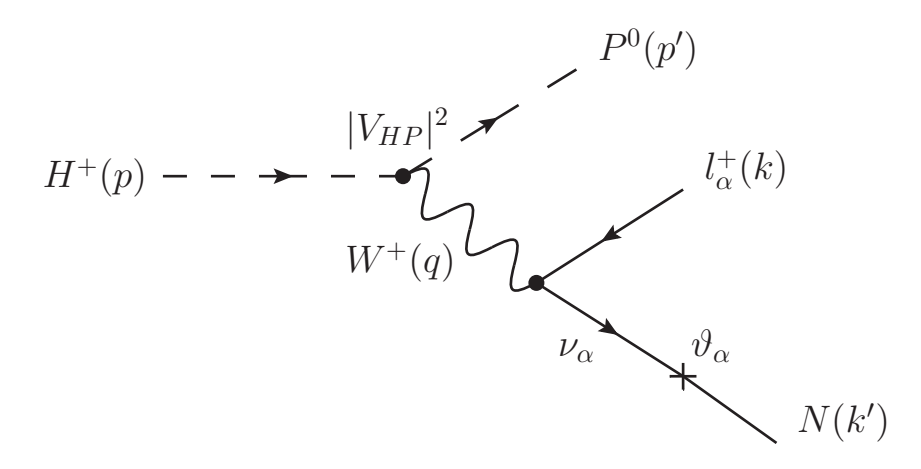


**Figure B.5:** The Feynman diagram for semi-leptonic decay of pseudo-scalar meson  $H^+ \to P^0 l_\alpha^+ N$  decay

The computation for three body pseudo-scalar meson decays from Figure B.5 is somewhat more complicated. It involves the leptonic part, which is calculable using the Fermi theory, and hadronic part, which involves the transition of confined quarks. The amplitude for the process takes the following form [34]

$$iM = \frac{G_F V_{qq'}^*}{\sqrt{2}} \vartheta_{\alpha} \bar{u}^s(k) \gamma_{\mu} (1 - \gamma^5) u^{s'}(k') \cdot \langle P | \bar{q}' \gamma^{\mu} (1 - \gamma^5) q | H \rangle$$
 (B.33)

The hadronic part can be parameterized in the following way

$$\langle P|\bar{q}'\gamma^{\mu}(1-\gamma^{5})q|H\rangle = (p+p')^{\mu}f_{+}(q^{2}) + (p-p')^{\mu}f_{-}(q^{2})$$
 (B.34)

Here  $f_+(q^2)$  and  $f_-(q^2)$  are the form factors, which can be approximated as

$$f_{\pm}(q^2) = \frac{f_{\pm}(0)}{1 - q^2 / M_{pol}^2}$$
 (B.35)

where  $f_+(0)$  and  $f_-(0)$  are constants associated with the decaying meson and  $M_{pol}$  can be approximated with the mass of nearest resonance to H with same  $I^P$  as the hadronic weak current responsible for  $q \to q'$  quark

transition. After somewhat longer calculation the differential branching ratio can be shown to equal [31]

$$\frac{\mathrm{d}Br(H \to P \, l_{\alpha}^{+} \, N)}{\mathrm{d}E_{N}} = \frac{G_{F}^{2} |V_{qq'}|^{2}}{64\pi^{3}\tau_{H}M_{H}^{2}} \vartheta_{\alpha}$$

$$\cdot \int \mathrm{d}q^{2} \left[ f_{-}^{2}(q^{2}) \cdot \left( q^{2}(M_{N}^{2} + M_{l}^{2}) - (M_{N}^{2} - M_{l}^{2})^{2} \right) \right]$$

$$+ 2f_{+}(q^{2})f_{-}(q^{2}) \left( M_{N}^{2}(2M_{H}^{2} - 2M_{H}^{2} - 4E_{N}M_{H} - M_{l}^{2} + M_{N}^{2} + q^{2}) + M_{l}^{2} - M_{N}^{2} - q^{2} \right)$$

$$+ f_{+}^{2}(q^{2}) \left( (4E_{N}M_{H} + M_{l}^{2} - M_{N}^{2} - q^{2})(2M_{H}^{2} - 2M_{H}^{2} - 4E_{N}M_{H} - M_{l}^{2} - M_{N}^{2} - q^{2}) - (2M_{H}^{2} + 2M_{H} - q^{2})(q^{2} - M_{N}^{2} - M_{l}^{2}) \right) \right]$$
(B.36)

Here  $V_{qq'}$  is the CKM matrix element corresponding to the quark transition and  $\tau_H$  the  $H^+$  meson's lifetime.

# References

- [1] S. Weinberg, *A Model of Leptons*, Physical Review Letters **19**, 1264 (1967).
- [2] E. Akhmedov, Majorana neutrinos and other Majorana particles: Theory and experiment, arXiv.org 1412.3320.
- [3] T. Asaka and M. Shaposhnikov, *The v MSM*, dark matter and baryon asymmetry of the universe, Physics Letters B , 1 (2005).
- [4] E. K. Akhmedov, V. A. Rubakov, and A. Y. Smirnov, *Baryogenesis via neutrino oscillations*, Physical review letters , 5 (1998).
- [5] L. Canetti, M. Drewes, T. Frossard, and M. Shaposhnikov, *Dark Matter, Baryogenesis and Neutrino Oscillations from Right Handed Neutrinos*, Phys.Rev. **D87**, 93006 (2013).
- [6] B. Pontecorvo, *Neutrino Experiments and the Problem of Conservation of Leptonic Charge*, Soviet Journal of Experimental and Theoretical Physics **26**, 984 (1968).
- [7] D. S. Gorbunov and V. A. Rubakov, *Introduction to the Theory of the Early Universe*, World Scientific Publishing Company, 2011.
- [8] M. C. Gonzalez-Garcia, M. Maltoni, and T. Schwetz, *Updated fit to three neutrino mixing: status of leptonic CP violation*, nu-fit.org (2014).
- [9] M. Gonzalez-Garcia, M. Maltoni, and T. Schwetzd, *NuFIT 2.0: Three-neutrino results after the NOW 2014 Conference*, nu-fit.org (2014).
- [10] Y. Fukuda et al., Measurement of the Flux and Zenith-Angle Distribution of Upward Throughgoing Muons by Super-Kamiokande, Physical Review Letters 82, 2644 (1999).
- [11] F. P. An et al., Spectral Measurement of Electron Antineutrino Oscillation Amplitude and Frequency at Daya Bay, Physical Review Letters 112, 061801 (2014).

70 References

[12] O. Ruchayskiy and A. Ivashko, *Experimental bounds on sterile neutrino mixing angles*, Journal of High Energy Physics **2012**, 18 (2012).

- [13] A. Atre, T. Han, S. Pascoli, and B. Zhang, *The Search for Heavy Majorana Neutrinos*, Journal of High Energy Physics **0905**, 60 (2009).
- [14] R. E. Shrock, General theory of weak processes involving neutrinos. II. Pure leptonic decays, Physical Review D **24**, 1275 (1981).
- [15] M. Aoki et al., Search for massive neutrinos in the decay  $\pi \rightarrow \nu$ , Physical Review D **84**, 5 (2011).
- [16] D. I. Britton, S. Ahmad, D. A. Bryman, R. A. Burnham, E. T. H. Clifford, P. Kitching, Y. Kuno, J. A. Macdonald, T. Numao, A. Olin, J. M. Poutissou, and M. S. Dixit, *Improved search for massive neutrinos in*  $\pi$  +  $\rightarrow$  e +  $\nu$  decay, Physical Review D **46**, R885 (1992).
- [17] A. V. Artamonov et al., Search for heavy neutrinos in  $K \rightarrow \mu + \nu$  decays, Physical Review D **91**, 1 (2015).
- [18] R. Hayano, T. Taniguchi, T. Yamanaka, T. Tanimori, R. Enomoto, A. Ishibashi, T. Ishikawa, S. Sato, T. Fujii, T. Yamazaki, S. Kurokawa, S. Schnetzer, and Y. Takada, *Heavy-Neutrino Search Using K μ Decay*, 1982.
- [19] K. and others Yamazaki, T. and Ishikawa, T. and Akiba, Y. and Iwasaki, M. and Tanaka, *Search for Heavy Neutrinos in Kaon Decay*, Conf.Proc. **C840719**, I.262 (1984).
- [20] G. Bernardi, G. Carugno, J. Chauveau, and F. Dicarlo, *Search for neutrino decay*, Physics Letters B **166**, 479 (1986).
- [21] G. Bernardi, G. Carugno, J. Chauveau, and F. Dicarlo, *Further limits on heavy neutrino couplings*, Physics Letters B **203**, 3 (1988).
- [22] F. Bergsma et al., A search for decays of heavy neutrinos, Physics Letters B 128, 361 (1983).
- [23] J. Dorenbosch et al., A search for decays of heavy neutrinos in the mass range 0.5–2.8 GeV, 1986.
- [24] A. Vaitaitis, Search for Neutral Heavy Leptons in a High-Energy Neutrino Beam, Physical Review Letters 83 (1999).
- [25] A. D. Dolgov, S. H. Hansen, G. Raffelt, and D. V. Semikoz, *Heavy sterile neutrinos: Bounds from big-bang nucleosynthesis and SN 1987A*, Nuclear Physics B **590**, 19 (2000).
- [26] A. D. Dolgov, S. H. Hansen, G. Raffelt, and D. V. Semikoz, *Cosmological and astrophysical bounds on a heavy sterile neutrino and the KARMEN anomaly*, Nuclear Physics B **580**, 30 (2000).

References 71

[27] A. D. Sakharov, Violation of CP invariance, C asymmetry, and baryon asymmetry of the universe, Soviet Physics Uspekhi 34, 392 (1991).

- [28] A. Kusenko, S. Pascoli, and D. Semikoz, *Bounds on heavy sterile neutrinos revisited*, Journal of High Energy Physics **2005**, 028 (2005).
- [29] S. Alekhin, W. Altmannshofer, T. Asaka, B. Batell, F. Bezrukov, K. Bondarenko, A. Boyarsky, N. Craig, B. Gavela, G. F. Giudice, D. Gorbunov, and S. Gori, *A facility to Search for Hidden Particles at the CERN SPS : the SHiP physics case*, arXiv.org **1504.04855** (2015).
- [30] G. L. Fogli, E. Lisi, A. Marrone, D. Montanino, and A. Palazzo, *Getting the most from the statistical analysis of solar neutrino oscillations*, Physical Review D **66**, 21 (2002).
- [31] D. Gorbunov and M. Shaposhnikov, *How to find neutral leptons of the nuMSM*?, Journal of High Energy Physics **10**, 45 (2007).
- [32] K. Olive, Review of Particle Physics, Chinese Physics C 38, 090001 (2014).
- [33] M. Peskin and D. Schroeder, *An introduction to quantum field theory*, Addison-Wesley Publishing Company, 1995.
- [34] S. Aoki et al., Review of lattice results concerning low energy particle physics, arXiv.org 1310.8555 (2013).